

DETERMINING CRITICAL RESIDUES FOR INTERSUBUNIT BINDING OF THE HUMAN  
EPITHELIAL SODIUM CHANNEL

THESIS

Presented to the Graduate Council of  
Texas State University-San Marcos  
in Partial Fulfillment  
of the Requirements

for the Degree

Master of SCIENCE

By

Grantham C. Peltier, B.S.

San Marcos, Texas  
August 2012

DETERMINING CRITICAL RESIDUES FOR INTERSUBUNIT BINDING OF THE HUMAN  
EPITHELIAL SODIUM CHANNEL

Committee Members Approved:

---

Wendi M. David, Chair

---

Rachell E. Booth

---

Steven T. Whitten

Approved:

---

J. Michael Willoughby  
Dean of the Graduate College

**COPYRIGHT**

By

Grantham C. Peltier

2012

## **FAIR USE AND AUTHOR'S PERMISSION STATEMENT**

### **Fair Use**

This work is protected by the Copyright Laws of the United States (Public Law 94-553, section 107). Consistent with fair use as defined in the Copyright Laws, brief quotations of this material are allowed with proper acknowledgement. Use of this material for financial gain without the author's express written permission is not allowed

### **Duplication Permission**

As the copyright holder of this work I, Grantham C. Peltier, refuse permission to copy in excess of the "Fair Use" exemption without my written permission.

## **ACKNOWLEDGEMENTS**

I would like to thank all of my committee members for their help during this project. Special appreciation is given to Dr. Wendi David for her guidance and insight into surface plasmon resonance, and Dr. Rachell Booth for the use of her laboratory and guidance. I would like to thank my family for all of their support throughout the whole process, with special gratitude to my loving wife for her support and patience. Additionally, I would like to thank Dr. Corina Maeder for her specific insights, and Dr. Kevin Lewis for providing materials to conduct this research. Finally I would like to thank Texas State University-San Marcos for providing me with the opportunity to pursue this project.

This manuscript was submitted on July 26<sup>th</sup>, 2012

## TABLE OF CONTENTS

	<b>Page</b>
ACKNOWLEDGMENTS.....	v
LIST OF TABLES .....	vii
LIST OF FIGURES .....	viii
CHAPTER	
I.    INTRODUCTION .....	1
II.   MATERIALS AND METHODS .....	13
III.  RESULTS AND DISCUSSION .....	25
IV.   CONCLUSION.....	47
REFERENCES .....	50

## LIST OF TABLES

<b>Table</b>	<b>Page</b>
1. Primer sequences of target residue peptides .....	13
2. Peptide sequences .....	22
3. Potentially important intersubunit contacts .....	32
4. E438 Kinetics.....	40
5. E254 Kinetics.....	41
6. Summary of Kinetics .....	47
7. Future targets .....	48

## LIST OF FIGURES

Figure	Page
1. Kidney and nephron .....	2
2. Predicted structure of hENaC .....	5
3. Predicted structure of $\alpha$ -hENaC.....	6
4. Surface plasmon resonance function and resultant data .....	9
5. General capture methods .....	11
6. Crystal structure of chicken ASIC 1 .....	26
7. Immobilization of WT-A7 .....	27
8. Immobilization of PEG-WT-A7 via insertion into dextran.....	28
9. Serial dilution of analyte against WT-A7.....	29
10. Derivatization of WT-A6 .....	30
11. Serial dilution of analyte against WT-A6.....	31
12. Digestion of vector .....	33
13. Insert and vector preparation .....	33
14. Ligation product digestion.....	34
15. Expression of GST-fusion peptides .....	36
16. Immobilization of ligand E438 .....	37
17. Binding assay against E438.....	38
18. Binding assay against E254.....	40

19. Free GST control assay .....	42
20. Non-specific interactions control assay .....	43
21. PIP <sub>2</sub> binding assay .....	45
22. Non-specific interactions binding assay against PIP <sub>2</sub> .....	45

## CHAPTER I

### Introduction

Sodium is a critical element in mammalian systems. Imbalance of the proper levels of sodium in a living organism can lead to dehydration, renal disease, and hypertension, among other problems (1). With serious consequence, it becomes obvious for the need to effectively regulate the osmotically active cation, sodium.

In mammals, sodium is reabsorbed into epithelial cells from the extracellular fluid near the apical membranes via the epithelial sodium channel (ENaC) (2). In order to understand more clearly the mechanism of sodium reabsorption by ENaC, structure/function studies are underway. This should give detailed clues about the regulation of sodium in living organisms.

#### **Epithelial Sodium Channel (ENaC)**

##### Significance:

The ENaC protein is part of the epithelial sodium channel/degenerin (ENaC/DEG) ion channel protein family (2). This is a group of nonvoltage-gated sodium channels with similar structural features. ENaC is localized in the apical membranes of

epithelial cells in the kidney, primarily the distal tubule collecting duct (**Figure 1**), and also the lung and colon (1). Sodium reabsorption occurs passively along a sodium concentration gradient through ENaC, and homeostasis is maintained in these cells through an active transport channel on the basolateral membrane that releases  $\text{Na}^+$  in exchange for  $\text{K}^+$  (1).

The function of ENaC is affected by various molecules, allowing for the regulation of  $\text{Na}^+$  reabsorption. Both amiloride (1) and triamterene (3) block the pore of ENaC leading to less effective sodium reabsorption. Down-regulation of sodium reabsorption is controlled primarily by channel retrieval of ENaC from the epithelial membrane,

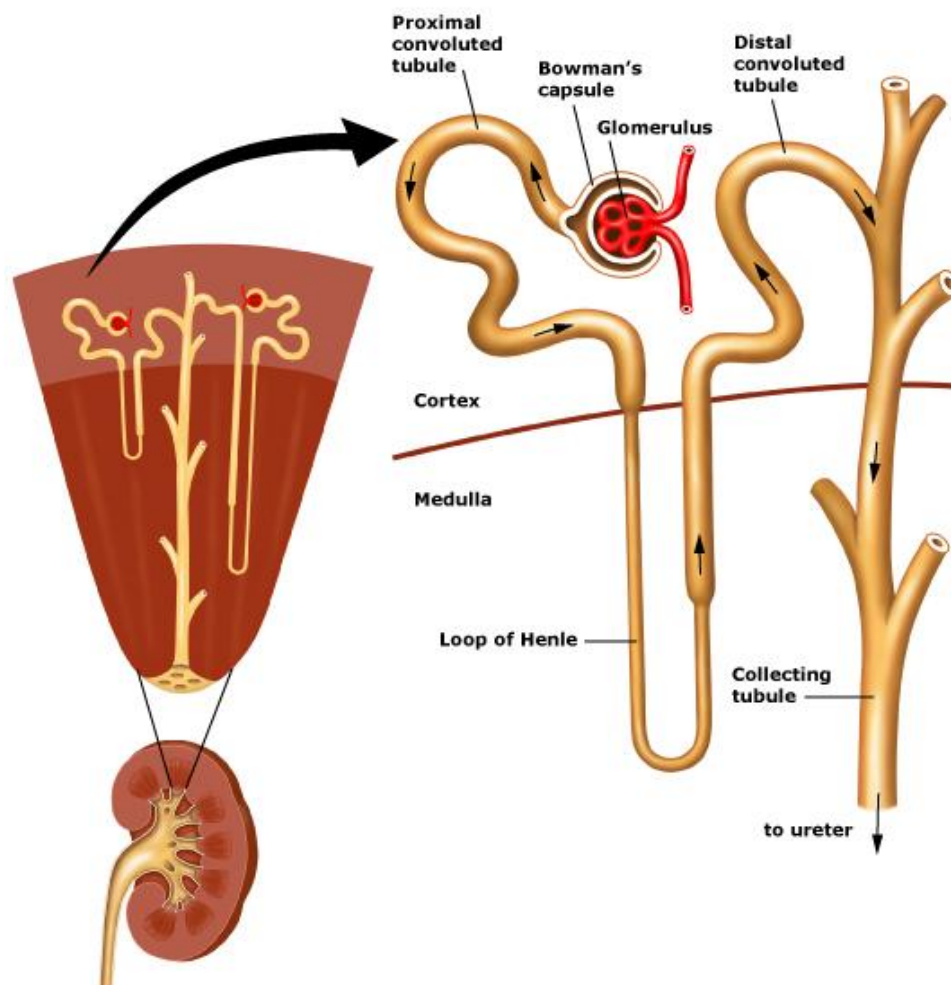


**Figure 1. Kidney and nephron.** Depiction of where primary  $\text{Na}^+$  reabsorption occurs (4).

through a process mediated by the E3 class ubiquitin – protein ligase Nedd4-2. Nedd4-2 binds to the carboxy-terminus of ENaC, signaling channel retrieval and ultimately leading to less sodium reabsorption (5). Up-regulation of ENaC activity is mediated by the mineralcorticoid aldosterone. Aldosterone signals the production of phosphatidylinositol 4, 5-trisphosphate (PIP<sub>2</sub>) through activation of phosphoinositide 3-OH kinase (PI3K) (6,7). PIP<sub>2</sub> leads to greater ENaC activity but whether or not a direct binding interaction occurs between PIP<sub>2</sub> and ENaC is not yet determined. The atrial natriuretic peptide (ANP) inhibits the activation of ENaC (8) through suppression of the rennin-angiotensin-aldosterone axis, which regulates the hormone aldosterone. In contrast, ANP has been seen to increase ENaC activity in the urinary bladder of the Japanese tree frog, through a yet undetermined mechanism (9).

As ENaC is the limiting factor in sodium reabsorption, the importance for proper ENaC function becomes apparent. When there is disruption of its proper function, the resulting imbalance can lead to the cause of diseases linked to fluid and electrolyte homeostasis disruption.

There have been several diseases linked with ENaC, including two rare monogenetic disorders associated with this protein. Liddle's syndrome is caused by the disruption of the ubiquitin ligase, Nedd4, regulation pathway (10). This results from a mutation in Nedd4's binding site on the C-terminus of ENaC. Less Nedd4-2 binding leads to less retrieval of ENaC from the membrane. This ultimately leads to too much sodium reabsorption into the cell from too many channels in the membrane, resulting in hypertension. Pseudohypoaldosteronism (PHA) type 1 is caused by a loss-of-function

mutation that hinders the effect of the hormone aldosterone, which would normally cause ENaC activation (11). This mutation leads to low sodium reabsorption, which in turn can cause hypotension. Also, there is an autosomal recessive hereditary disease called Cystic Fibrosis that has been found to be related to ENaC (11). It is thought that there is an interaction between a cystic fibrosis protein, cystic fibrosis transmembrane conductance regulator (CFTR), and ENaC that can cause the disease. A mutation in the CFTR gene may lead to a gain-of-function mutation in ENaC. In contrast, it has been found that atypical cystic fibrosis can be caused by a loss-of-function mutation in the  $\beta$ -subunit of ENaC, leading to the symptoms of atypical cystic fibrosis (11). Study of the structure of the epithelial sodium channel will provide insight into the mechanisms of these known diseases and may ultimately provide methods for combating them.

#### Structure:

ENaC is a highly  $\text{Na}^+$ -selective pore-forming complex comprised of three subunits ( $\alpha$ ,  $\beta$ , and  $\gamma$ ) (12) (**Figure 2** and **3**). Previous studies have found that the heteromeric ENaC (containing all three subunits) has a much higher activity than the homomeric protein or lesser heteromeric constructions of the protein (14). This provides evidence that each individual subunit plays an important role in the mechanism of activity for ENaC.

Three conserved structural domains have been identified in the subunits of ENaC: two membrane-spanning domains referred to as TM1 and TM2; an extracellular loop, comprising over sixty percent of the protein, with several conserved cysteine

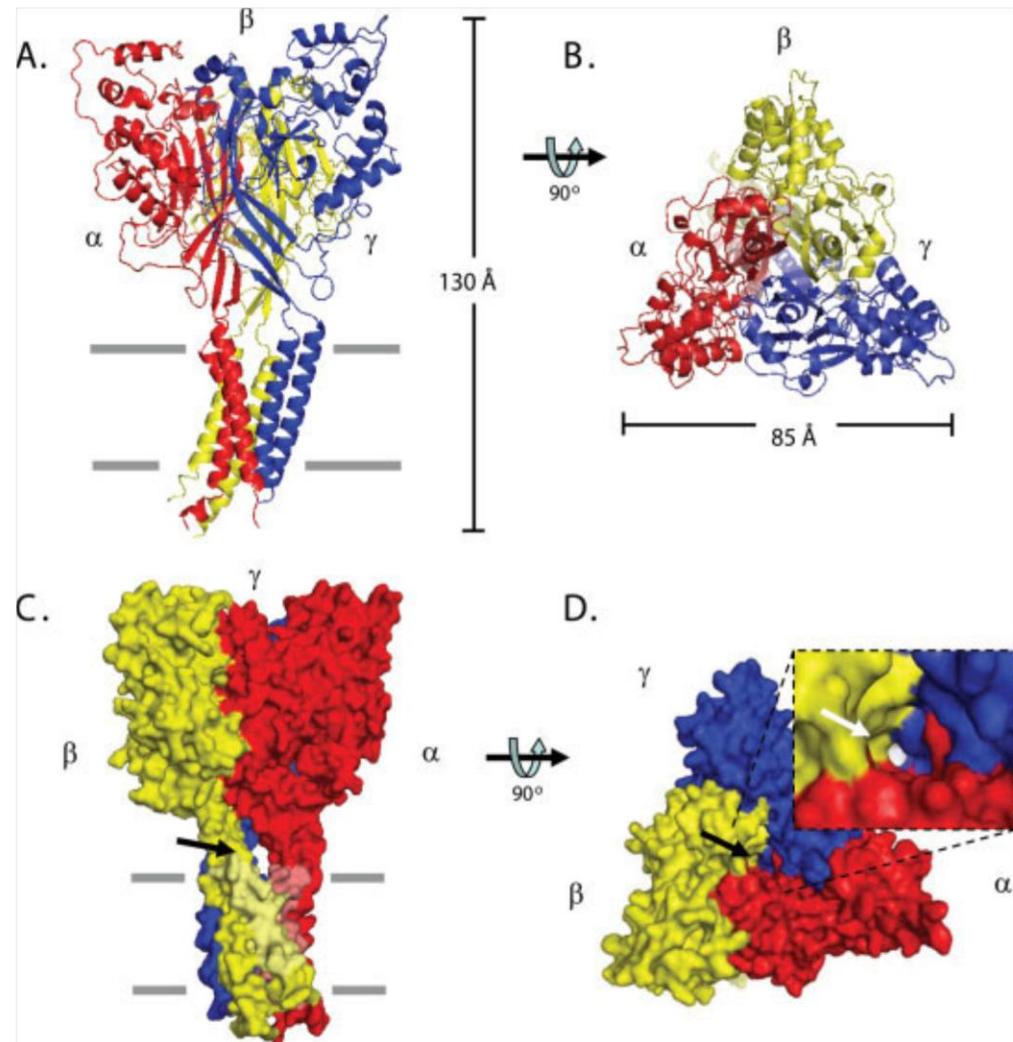


**Figure 2. Predicted structure of hENaC.** Subunit legend:  $\alpha$  – red,  $\beta$  – yellow,  $\gamma$  – blue. A) Ribbon structure viewed from the side. B) Ribbon structure viewed from above. C) Spatial filled model viewed from the side. Arrow noting cavities formed between transmembrane regions. D) Spatial filled model viewed from above. Enlarged portion shows the formed pore. (14)

residues; and a short N-terminus and C-terminus protruding into the cytosol (14). The conceptual flow from N- to C-termini would follow cytoplasmic N-terminus transmembrane into a large extracellular loop, then a final transmembrane to cytoplasmic C-terminus, near the N-terminus.

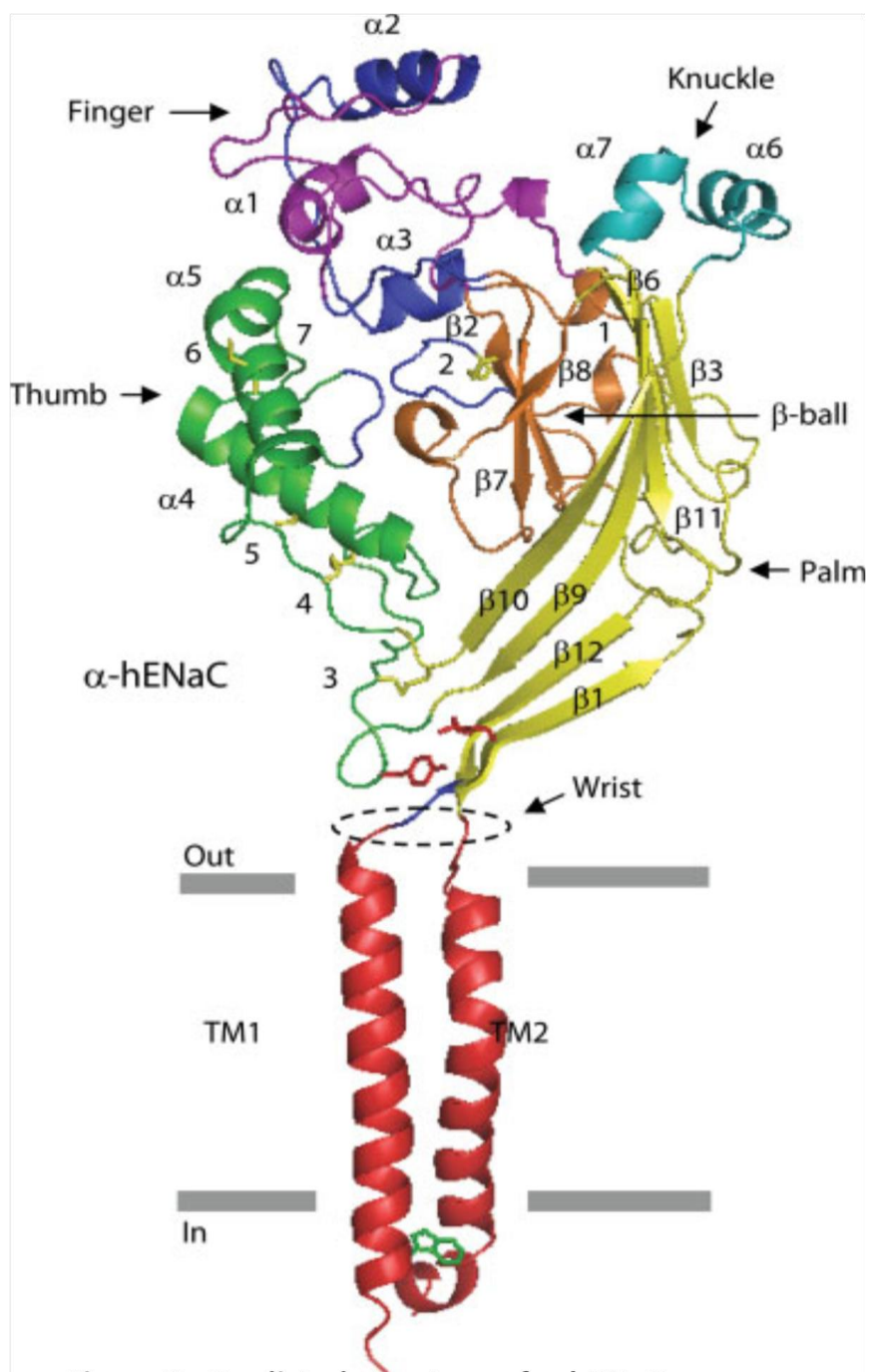


**Figure 3. Predicted structure of  $\alpha$ -hENaC.**

Similarly, each subunit would contain the observed domains: a thumb of 2 alpha helices, a finger of 3 short alpha helices, a knuckle of 2 short alpha helices, a palm of beta sheets, and a beta-ball. Also shown are the membrane spanning domains TM1 and TM2, the extracellular loop, and the cytoplasmic N- and C-termini (14).

Though a crystal structure for ENaC is not yet available, a prediction has been made via the sequence and structural similarities between ENaC and the ENaC/DEG family ion channel, cASIC1 (**Figure 2**) (14).

There are variations of ENaC containing a  $\delta$  subunit that has a high homology to  $\alpha$  subunit, rather than  $\beta$  or  $\gamma$ . These variant subunits can form trimers in the form of  $\delta$ ,  $\beta$ , and  $\gamma$ -ENaC and are found in the pancreas, testes, ovaries, and other non-epithelia cells, though specific function of these variant homologues is still uncertain (15).

The acid-sensing ion channel (ASIC) proteins belong to the ENaC/DEG family and thus hold several structural similarities with ENaC. This, combined with the recent discovery of the crystal structure of chicken ASIC 1, are reasons for using cASIC1 as a template for the prediction of ENaC structure (16). The crystal structure of cASIC1 shows the model of subunits as shown above, except that it is shown to be a homotrimer, rather than the heteromeric structure of ENaC. The protein cASIC1 serves as a framework structure for multiple proteins in the ENaC/DEG family, and is proving to be important in the study of the structure and function of the ENaC/DEG family proteins (17). The group responsible for the cASIC1 structure is also responsible for naming the domains shown in **Figure 3** (finger, thumb, palm, etc.), and has proposed that a conserved tryptophan residue in the thumb is used to transmit information about binding of a proton to the transmembrane domain, signaling for changes in the pore.

In order to determine interactions necessary for proper ENaC structure and function, two projects are underway. One project involves using a yeast screen to

identify gain- or loss-of-function ENaC mutants generated through random mutagenesis. Changes in function would potentially identify ENaC regions to focus our attention towards, through identification of the mutated ENaC residues. At the same time, a binding interaction screen will be developed to analyze intersubunit binding interactions utilizing surface plasmon resonance. Although the two projects are synergistic in nature, the focus of the work described in this thesis is the binding interaction screen for intersubunit binding interactions.

### **Surface Plasmon Resonance**

Surface plasmon resonance (SPR) is a spectroscopy technique that has been shown to have a great efficacy for binding studies. Binding interactions can be measured in a quantifiable manner, leading to determination of on and off rates for a specific interaction, as well as  $K_A$  and  $K_D$  values (18).

A proportional relationship between a shift in the angle of reflected light at a gold sensor surface and a binding interaction at the surface is the basis for SPR measurements (**Figure 4**). When a binding event between an immobilized ligand and a free analyte in solution occurs, the angle of the reflected light at the sensor surface is shifted, allowing quantitation of the extent of interaction. Once binding takes place, one can see an almost instantaneous change in the projected graph of the response units (RU), which are a computational conversion of reflection angle, and time.

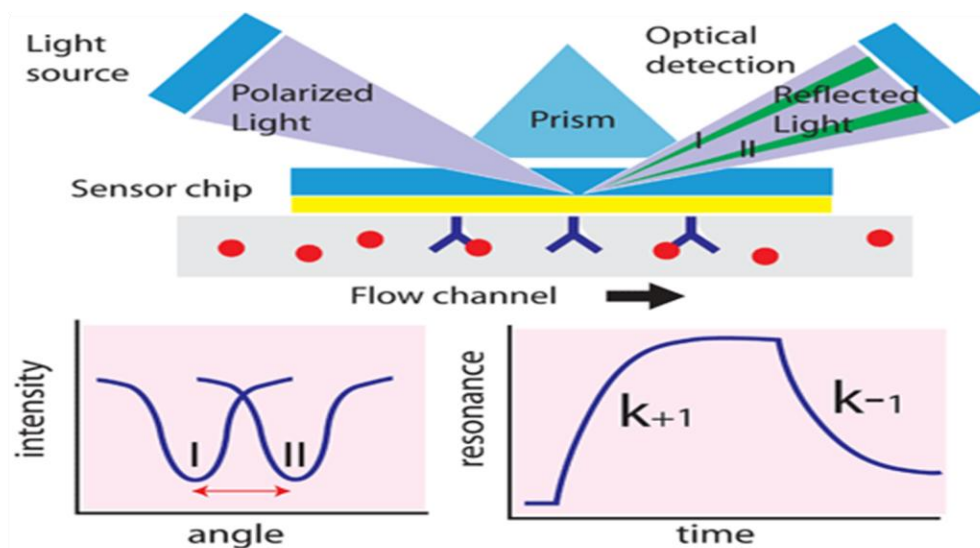


**Figure 4. Surface plasmon resonance function and resultant data.** When binding occurs between analyte (represented by the red circles in the flow channel) and ligand (represented by the blue “Y” structures attached to the gold surface), the resulting proportional change of the angle of the reflected light is quantifiable (19).

The RU is equal to one picogram/millimeter<sup>2</sup>, but the specific relation to different molecules varies depending on the molecules’ specific polarizability, size, and density (20). This gives a very useful method for observing the real-time binding of substrate to ligand.

During the SPR process, an incident beam of plane-polarized light, of wavelength  $\lambda$ , is projected through a prism and is reflected off of a glass/metal film interface, where the film has a thickness of  $<\lambda$ , for total internal reflection (**Figure 4**). When the light passes through the air/glass barrier of the prism, a phenomenon called an evanescent wave is produced, which is a decaying wave with deteriorating wavelength. The evanescent wave deteriorates and strikes the glass/film barrier with the same wavelength as the film and the phenomenon of surface plasmon occurs through

excitation of free electrons in the film. Surface plasmon resonance is the oscillation of the free electrons of the surface back and forth across the surface at boundaries of very different optical density changes (such as glass – metal – water, as seen in **Figure 4**) at a frequency unique to the particular surface (21).

Binding studies are performed via this technique due to its ability to detect small changes in mass of the bound ligands. When a substrate (analyte) binds to an immobilized ligand, it causes a change in the plasmon frequency, which subsequently alters the angle of reflection of the reflected light, in a manner proportional to the mass of the substrate bound to the ligand (18).

### **Goals of Project**

The purpose of this project was to identify critical binding interactions between the human ENaC (hENaC) subunits that may be necessary for functional ENaC protein. The current work focused on determination of ENaC intersubunit interactions using SPR.

In order to achieve the goals of this project, a general strategy scheme was used:

1. Select residues from predicted ENaC intersubunit regions
2. Express peptides containing selected residues
3. Immobilize peptides onto a SPR sensor chip

#### 4. Conduct binding assays for interactions between peptide regions

Simultaneously, point mutants were also identified in the yeast screen performed by colleagues in the Booth lab at Texas State. The yeast screen included the random point mutagenesis of mouse ENaC subunits in yeast cells, followed by tests for ENaC function. Mutations found in the yeast screen to lead to sodium insensitivity were utilized to identify candidate intersubunit peptide regions of ENaC that may be important for function. Once the target peptide regions were identified, the peptide binding partners were immobilized using different sensor surface immobilization strategies, depending on the particular experiment (**Figure 5**).

#### Summary

Epithelial sodium channels are a part of the epithelial sodium channel/degenerin family, and regulate sodium levels in mammalian organisms (1), but little information is available on ENaC structure. Recently, the crystal structure of another protein of the ENaC/DEG family, chicken acid-sensing ion channel 1, was determined (16). As the two

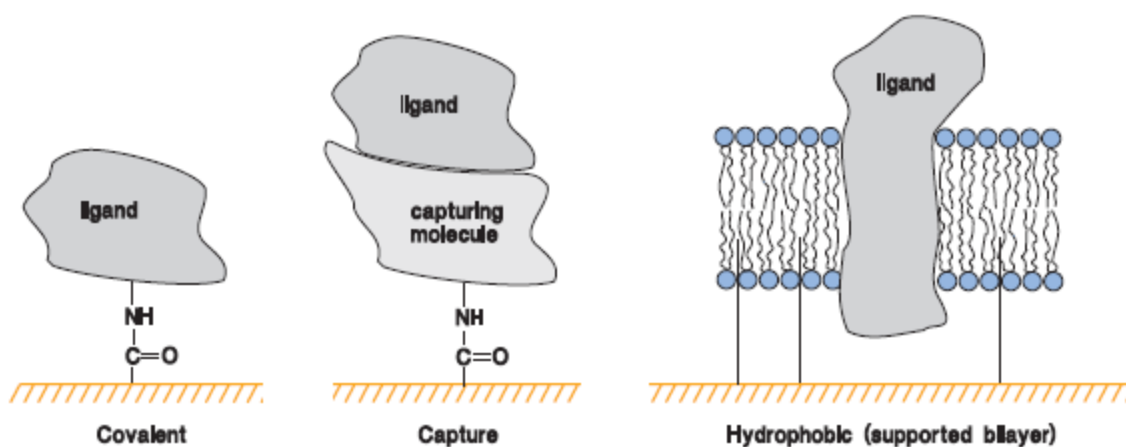


**Figure 5. General capture methods.** Shown are typical methods to capture ligands to the surface of a sensor chip (22).

proteins are quite similar, Stockand and Booth proposed a structure for ENaC based on cASIC1 (14). Using the proposed hENaC structure as a basis, as well as results from a functional ENaC yeast screen, peptide regions were identified that could potentially contribute to intersubunit structural interactions. Determination of the binding interactions by SPR will lead to a better understanding of overall ENaC structure.

## CHAPTER II

### MATERIALS AND METHODS

Chemicals and reagents: All reagents for buffer solutions were obtained from Sigma-Aldrich or GE Healthcare unless otherwise noted. A working stock solution of 10x concentrated HBS-EP buffer (0.1 M HEPES, 30 mM EDTA) was created for preparation of additional running buffers for experimental trials. Any modification to this buffer stock solution is noted in the individual method. All buffers were passed through 0.2 mm filters (Nalgene) and degassed for a minimum of ten minutes after buffer filtration.

**Table 1. Primer sequences of target residue peptides.** Underlined sequence signifies target ENaC sequence. Highlighted sequence shows restriction enzyme recognition sequences, with “GGATCC” for BamH I and “GCGGCCGC” for Not I. Unlabeled sequence is random nucleotides for restriction enzyme seating. T<sub>m</sub>'s were calculated using NEB's T<sub>m</sub> calculator, only using underlined sequences in the calculation. Forward and reverse primers are labelled with F and R, respectively.

Target Residue	Primers Sequence	T <sub>m</sub> (°C)
β-N-terminus	F: 5'-C <b>GGATCC</b> <u>ATG CACGTG AAG AAG TAC CTG AAG GG</u> -3'	68
	R: 5'-ATAAGAAT <b>GCGGCCGC</b> <u>GGC TTT CTT CTT GGG CC</u> -3'	62
α-Asn285	F: 5'-C <b>GGATCC</b> <u>GAG GAC ACG CTG GGCAAC TTCATC</u> -3'	74
	R: 5'-ATAAGAAT <b>GCGGCCGC</b> <u>GTG GAA GTG AGAGTA ATT CGCC</u> -3'	70
β-Glu438	F: 5'-C <b>GGATCC</b> <u>AACCGG GACTTC CCA GACTG</u> -3'	68
	R: 5'-ATAAGAAT <b>GCGGCCGC</b> <u>GGA CTC CTT GCA CAT GC</u> -3'	65
β-Glu254	F: 5'-C <b>GGATCC</b> <u>AGCTAC CCC GGCGAG CAG ATG ATC</u> -3'	75
	R: 5'-ATAAGAAT <b>GCGGCCGC</b> <u>GTA GAA GAT GGA CGT GAA GTT CCG</u> -3'	69
γ-Gln444	F: 5'-C <b>GGATCC</b> <u>TACCAG CAG CACCCC AACTG</u> -3'	71
	R: 5'-ATAAGAAT <b>GCGGCCGC</b> <u>GGC TTC CTT GCA CACAGAC</u> -3'	70

Primers: Primers were designed to incorporate cut sites for the restriction enzymes Not I and BamH I and were purchased from Integrated DNA Technologies (IDT, San Jose, CA). The forward direction primers contained a restriction enzyme seat for stability during digestion, the BamH I recognition sequence, and the sequence of the start of the target DNA sequence. Likewise, the reverse direction primers contained a restriction enzyme seat, the Not I recognition sequence, and the complementary sequence of the end of the target DNA sequence (**Table 1**).

PCR of insert DNA: Peptide DNA sequences were prepared via polymerase chain reaction (PCR) utilizing the primers (**Table 1**), the proofreading polymerase “Phusion” (optimum elongation temperature at 72 °C) from New England Biolabs (NEB, Ipswich, Massachusetts), 1X phusion GC reaction buffer from NEB, and hENaC gene individually inserted into pSWICK vectors (23). GC reaction buffer was used because of the high primer Tm’s. PCR was run on an Applied Biosystems GeneAmp® PCR system 2700, with two programs for dichotomy of Tm values (**Table 1**). A 3-step program was used for samples E438 and N-terminal tail (NT): 95 °C for 30 seconds, 65 °C for 30 seconds, then 72 °C for 30 seconds; ran for 35 cycles, and finished with a step of 72 °C for 10 minutes. A 2-step program was run for samples Q444, E254, and N285: 95 °C for 30 seconds, then 72 °C for 1 minute; ran for 35 cycles, and finished with a step of 72 °C for 10 minutes. Additional rounds of PCR were run using Clontechs’ 1X Advantage® 2 Polymerase mix (containing Taq and a proof-reading polymerase) and 1X Advantage® 2 PCR Buffer which have an optimum elongation temperature at 68 °C. Separate thermocycle programs

were run for the Advantage mix. A 3-step program for E438 and NT was used: 95 °C for 30 seconds, 65 °C for 30 seconds, then 68 °C for 30 seconds; ran for 35 cycles, and finished with a step of 68 °C for 10 minutes. Similarly, a 2-step program was run for samples Q444, E254, and N285: 95 °C for 30 seconds, then 68 °C for 1 minute; ran for 35 cycles, and finished with a step of 68 °C for 10 minutes. The PCR products were ethanol precipitated and combined for increased concentration.

*Horizontal gel electrophoresis:* Powdered agarose (OmniPur®) was dissolved in 1X TAE (40 mM Tris, 20 mM acetic acid, and 1 mM EDTA) buffer at approximately 1% w/v agarose, and heated in a microwave until completely dissolved. The gel solution was then cooled until warm to the touch, and 3.5 µL of ethidium bromide (final concentration of 44 ng/mL) was added. After a gentle mixing by swirling, the gel was poured into a cast and allowed to further cool and set. Once set, the gel was run in 1X TAE buffer at 120V for approximately 75 minutes. The DNA samples were mixed with 1X Loading Dye (NEB) and run next to a 1 kilobase ladder (NEB) for comparison. The gels were visualized under UV light and an image was captured with Alpha Innotech red™.

*Digestion:* The PCR products and the vector pGEX-4T-2 were digested with Not I and BamH I in NEB buffer 3. The vector, pGEX-4T-2 (GE Healthcare, Pittsburgh, PA) was chosen due to its inclusion of glutathione S-transferase (GST) and a thrombin cleaving site just at the end of GST. This provided a method of purification and immobilization with the utilization of anti-GST antibodies. The digestions proceeded at 37 °C for 2 hours, in a Baxter Scientific Products Durabath™ Water Bath.

The digested vector was treated using Antarctic Phosphatase and 1X Antarctic Phosphatase Reaction Buffer (NEB) to remove 5'-phosphates. Antarctic phosphatase is stable in NEBuffer 3 so no extra separation techniques were required. The reaction was incubated at 37 °C for 20 minutes. The phosphatase was heat inactivated by incubating at 65 °C for 5 minutes. The vector was cleaned through horizontal gel electrophoresis and gel extraction via QIAquick® Gel Extraction Kit (QIAGEN, Valencia, CA).

Ligation: Ligation of vector and insert was performed using T4 DNA Ligase with 1X T4 DNA Ligase Buffer (NEB). The reaction was performed at a 1:3 vector to insert ratio, and incubated for 20 minutes at room temperature.

Transformation into Top 10™ Competent Cells: The ligation products were then transformed into Top 10™ competent *E. coli* cells. Transformation for Top 10 cells followed a protocol modified from Chung and Miller (24). The competent cells were thawed on ice and then mixed with  $\geq 1$   $\mu$ g of DNA and incubated on ice for 20 minutes. Next, the reaction was heat shocked for 1 minute in 42 °C water bath, then back on ice for 2 minutes. One milliliter of preheated LB broth was added to the reaction and then incubated in a shaker at 37 °C and 225 rpm for 1 hour. The solution was spread on an LB/Amp agar plate and incubated overnight at 37 °C.

Transformation into BL21 cells: This transformation was performed via another modified protocol from Chung and Miller (24). A culture from the Top 10™ transformation was selected and grown in an overnight inoculation of LB broth supplemented with Amp and prepped with QIAGEN's QIAprep® Spin Mini-prep Kit. The BL21 cells were thawed on ice for 10 minutes, and then cold KCM buffer was added to

the cells at a 1:1 ratio with 5  $\mu$ L of DNA. This solution was incubated on ice for 20 minutes. Next, the solution was incubated, floating, in a room temperature water bath for 10 minutes. SOC (0.9 mL) was added to the transformation solution, and incubated at 37 °C with shaking at 225 rpm for 1 hour. The solution was spread on an LB/Amp agar plate and incubated overnight at 37 °C.

Expression: Expression was performed at mini-scale for clarification of proper expression, and then later, a full-scale expression for purification and use. Cell cultures were inoculated overnight in LB broth supplemented with Amp. The overnight culture was added to 2X-YTG/Amp media and then shaken for 3 hours at 37 °C and 225 rpm. At the end of the 3 hours, 0.1 mM IPTG (Promega, Fitchburg, WI) was added and the culture was incubated at 37 °C and 225 rpm for another 2.5-3 hours. The cells were spun down at 4600 X *g* for 5 minutes. The supernatant was discarded and the pellet frozen in a -80 °C freezer.

The pellet was thawed, PBS buffer (phosphate buffered saline, Mg<sup>2+</sup>, Ca<sup>2+</sup>; 0.2 g/L KCl, 0.2 g/L KH<sub>2</sub>PO<sub>4</sub>, 8 g/L NaCl, 1.15 g/L anhydrous NaHPO<sub>4</sub>, pH 7.4) was added (50  $\mu$ L PBS/ 1 mL culture) and the pellet was resuspended. The cells were put through two more freeze/thaw cycles to complete cell lysis. The solution was treated with 2  $\mu$ g/mL Deoxyribonuclease 1 (Sigma), and incubated at 37 °C for 30 minutes. The solution was then clarified by centrifugation (Beckman-Coulter Allegra™ 25R Centrifuge; Microfuge® 18 Centrifuge) at 10,500 X *g* for 20 minutes: the supernatant was saved.

SDS-PAGE: SDS-PAGE was run using NuPAGE® 10% Bis-Tris Gel, 1.0 mm X 12 well, in 1X NuPAGE® MES SDS running buffer (Invitrogen, Carlsbad, CA). The samples were

prepared using NuPAGE® 1X LDS Sample Buffer, and incubated at 70-75 °C for 10 minutes to denature the proteins. The gel electrophoresis was set up in an Invitrogen Novex® Mini-Cell with an XCell SureLock™ lid. The gel was run at a constant 200V for 35 minutes, using PageRuler™ Prestained Protein Ladder (Thermoscientific, Dubuque, IA) as a molecular weight standard and an E-C Apparatus Corporation EC3000P Series 90 Programmable power supply.

Western Blot: A western blot was performed to clarify that appropriate expression was achieved. The transfer to nitrocellulose membrane took place in a BIO-RAD (Hercules, CA) Mini Trans-Blot® Cell onto BIO-RAD Trans-Blot® Transfer Medium (0.45 µm) in a nitrocellulose sandwich (anode -> pad -> filter paper -> SDS-PAGE gel -> nitrocellulose membrane -> filter paper -> pad -> cathode) at 100V for 1 hour using a BIO-RAD PowerPac HC™ 250V/3.0A/300W power supply. The membrane was blocked with blocking solution of TBST [1X TBS (BIO-RAD), 0.1% Tween20 (Promega)], and 5% w/v dry milk; this incubated for 30 minutes at room temperature with rocking. Primary antibody (Rabbit Anti-GST from Invitrogen) was applied to the membrane and incubated overnight at 4 °C (4 µL antibody / 1 mL blocking solution from a 250 µg/mL stock). After three 10 minute washes with 40-50 mL of 1X TBST (with rocking), the secondary antibody (Peroxidase-labeled affinity purified antibody to Rabbit IgG (H+L) from (Kirkegaard & Perry Laboratories, Gaithersburg, MD) was applied with rocking at room temperature for 1 hour at a 1/20,000 dilution. The membrane was washed 3X more for 10 minutes each with TBST, and a final 10 minute wash of 1X TBS.

The GST proteins were visualized via X-ray film exposure using chemiluminescent substrates (Perkin Elmer Western Lightning® Plus – ECL) per manufacturer instructions. Film was exposed to blot for 1 minute and developed in an AFP Imaging Mini Medical 90. Fusion peptides were also visualized using Anti-Rabbit IgG (Fc) AP Conjugated (Promega, S373B) using a substrate solution: 10 mL of Alkaline Phosphatase buffer and 66  $\mu$ L of NBT, mixed well, then 33  $\mu$ L of BCIP added, and a final thorough mixing (BCIP/NBT from Promega). The blot was rinsed twice with alkaline phosphatase buffer, and the substrate solution was added allowed to incubate with gentle agitation on a rocker. The blot was allowed to develop for 10 minutes to an hour, as needed, then washed with distilled water for 10 minutes to stop the reaction.

Tris-Tricine vertical gel electrophoresis: Additionally, for lower molecular weight peptides, confirmation was achieved with a 20% Tris-tricine SDS-PAGE. The vertical gel was prepared using the protocol found in chapter 10 of Current Protocols in Protein Science (24), adjusted for 20% polyacrylamide (BIO-RAD). The separating gel was used at 20% polyacrylamide (10 mL 40% 29:1 acrylamide/bisacrylamide, 6.7 mL Tris-HCl/SDS buffer pH 8.45, 2.7 mL glycerol, 0.2 mL 10% w/v ammonium persulfate (Mallinckrodt AR®, Hazelwood, MO), 0.4 mL water, and 10.7  $\mu$ L TEMED(BIO-RAD)) with a 6% polyacrylamide stacking gel (1.3 mL 40% 29:1 acrylamide/bisacrylamide, 2.5 mL Tris-HCl/SDS buffer pH 8.45, 6 mL water, 20  $\mu$ L ammonium persulfate, and 12  $\mu$ L TEMED). Samples were mixed in Tris-Tricine sample buffer (4 mL water, 2 mL 0.5 M Tris-HCl buffer pH 6.8, 2.4 mL 50% glycerol, 1 mL 10% SDS (Shelton Scientific, Inc., Shelton, CT), 0.2 mL  $\beta$ -mercaptoethanol, and 2 mg Brilliant Blue R (Sigma-Aldrich) at a 2:1 ratio of

sample buffer to sample. The gel was run along with the protein ladder SeeBlue™ (Invitrogen, LC5625) at 100V for 2.5 – 3 hours and visualized by Coomassie stain.

Purification: Peptide purification was achieved via affinity chromatography, using a GST column with Thermoscientific's Pierce® Glutathione agarose as the stationary phase. The peptides were bound to 0.5 mL agarose by incubating on a rocker for 1 hour. The resin was allowed to settle, and the column was washed with 10 mL of 1X PBS. The resin was allowed to settle again and washed in that manner two more times. The resin was settled one more time and excess PBS was removed. GST-peptides were eluted using a 10 mM reduced glutathione in 50 mM Tris-HCl pH 8. This eluant was added to the column and mixed, then incubated at room temperature for 10 minutes. The column was drained and eluate was collected.

Thrombin cleavage of GST-fusion peptides: Peptides intended to be used as analytes in SPR binding studies were cleaved from GST with the protease Thrombin (GE Healthcare, product number 27-0846-01), following suggested usage from GE Healthcare. The GST-fusion peptides were bound to anti-GST sepharose and incubated at room temperature on a rocker for 1 hour. The GST-bound sepharose was washed 3x with PBS buffer, and incubated overnight at room temperature with Thrombin reaction mixture (50 µL thrombin stock and 950 µL PBS). PBS buffer was used to elute the cleaved peptides, which was collected in fractions. The thrombin was separated from cleaved peptide solution using *p*-AminoBenzamidine agarose (Sigma, product number A7155) following usage instructions provided by Sigma. One mL of agarose solution was added to the column and was washed 3 times with Tris buffer (50 mM Tris-HCl, 0.4 M

NaCl, pH 8.15) to remove preservatives. The cleaved peptide fractions were combined in the column and incubated overnight at 4 °C on a rocker, as suggested by Holleman and Weiss (25). Elution was performed with Tris buffer, and fractions were collected.

BCA assay: Expressed fusion-peptides were quantitated using a BCA Protein Assay Kit (Thermoscientific). The absorbance of BSA standards (1000, 500, 250, 125, 62.5, 31.3, and 0 µg/mL) was determined with a 96 well plate spectrophotometer (BIO-RAD iMark™ Microplate Reader) set at 590 nm. Samples were diluted to 1/10, and 25 µL of each was added to a corresponding well. BCA working solution was mixed (50 parts BCA reagent A: 1 part BCA reagent B), and 200 µL was added to each well. The plate was shaken for 30 seconds and incubated at 37 °C for 15 minutes before absorbance measurements. All BCA samples and standards were run in duplicate, and concentration values were averaged for the duplicates.

Tryptophan/tyrosine extinction coefficient concentration calculation: Cleaved peptide concentration was calculated from the following tryptophan/tyrosine extinction coefficient equation:

$$\frac{A_{280} * DF * MW}{(\#W * 5560) + (\#Y * 1200)} = Concentration$$

where  $A_{280}$  is the absorption at 280 nm, DF is the dilution factor of the sample, MW is molecular weight in mg/mole, #W is the number of tryptophans in the peptide, 5560 is the extinction coefficient of tryptophan at 280 nm at neutral pH in a 1 cm cell with units of AU/mole/mL, #Y is the number of tyrosines in the peptide, and 1200 is the extinction coefficient of tyrosine at 280 nm at neutral pH in a 1 cm cell with units

AU/mmol/mL. Cleaved peptide absorbance was obtained from BIO-RAD SmartSpec™ 3000 at 280 nm.

***Binding Assays:*** All binding assays were performed via SPR on a Biacore® X (GE Healthcare). The binding assays were conducted in HBS-EP running buffer (10 mM HEPES pH 7.4, 3 mM EDTA, 150 mM NaCl, 0.005% Volume/Volume Tween20) at 10  $\mu$ L/min, unless otherwise mentioned. The analyte peptides were injected in a series of serial dilutions at 50  $\mu$ L sample sizes.

Kinetic data calculations and sensorgram manipulation were done using BIAevaluation software version 2.3.

**Table 2. Peptide sequences.** Designed sequences for target residues. Bolded and underlined residues indicate the target residue

Peptide Name	Target Location	Peptide Sequence
WT-A6	$\beta$ -subunit $\alpha$ -helix 6	WPSE <b><u>E</u></b> ASEDWIFHV
Mut-A6	$\beta$ -subunit $\alpha$ -helix 6	WPS <b><u>G</u></b> ASEDWIFHV
WT-A7	$\alpha$ -subunit $\alpha$ -helix 7	NYTVNNKR <b><u>N</u></b> GVA
$\Delta$ NT	$\beta$ -subunit N-terminal tail	KRIICEGPKKKA
E438	$\beta$ -thumb	NRDFPDWAHCYSDLQMSVAQR <b><u>E</u></b> TCIGMCKES
N285	$\alpha$ -palm	EDTLGNFIFACR <b><u>F</u></b> NQVSCNQANYSHFH
E254	$\beta$ -palm	SYPGEQMILACLFGA <b><u>E</u></b> PCNYRNFTSIFY
Q444	$\gamma$ -thumb	YQQHPNWMYCYQLHRAFV <b><u>Q</u></b> EELGCQSVCKEA

Crystal structure identified peptide binding assay: Some peptides used in binding assays were purchased from Genescript: Mut-A6, WT-A6, WT-A7 (purchased with a conjugated N-terminal linker PEG2000 [polyethylene glycol with molecular weight of 1800-2200]) (**Table 2**). The peptide WT-A7 was immobilized onto a CM5 chip via amine coupling. The procedure was conducted according to the suggested protocol by GE Healthcare (22): the chip surface was activated with a 1:1 mixture of 0.5 M 1-ethyl-3-(3-dimethylaminopropyl)carbodiimide (EDC) and 0.1 M *N*-hydroxysuccinimide (NHS) [70  $\mu$ L injection at 10  $\mu$ L/min]; the ligand was loaded [70  $\mu$ L injection at 10  $\mu$ L/min]; the chip surface was deactivated with 1 M Ethanolamine-HCl pH 8.5 [70  $\mu$ L injection at 10  $\mu$ L/min].

Crystal structure identified peptide binding assays: Peptides WT-A6 and Mut-A6 were assayed against the immobilized peptide WT-A7 in a serial dilution of concentrations ( $1.6 \times 10^{-3}$  M,  $8.3 \times 10^{-4}$  M,  $4.2 \times 10^{-4}$  M,  $2.1 \times 10^{-4}$  M,  $1.0 \times 10^{-4}$  M, and  $5.2 \times 10^{-5}$  M) at a flow of 10  $\mu$ L/min in HBS-EP running buffer.

Anti-GST immobilization: The GST-Antibody was immobilized onto two flow cells of a CM5 chip through amine coupling using an Amine Coupling Kit and GST Capture Kit from GE Healthcare. The chip surface was activated with a 1:1 EDC/NHS solution injection of 35  $\mu$ L at 5  $\mu$ L/min for a 7 minute contact time. Anti-GST (provided in GST Capture Kit) was diluted to 15  $\mu$ g/mL and used in an injection of 25  $\mu$ L for a 5 minute contact time. When the desired RU change was obtained (indicating the amount of immobilized anti-GST), the chip surface was deactivated with a 35  $\mu$ L injection of ethanolamine for a 7 minute contact time. High affinity sites on anti-GST were blocked

using 5 µg/mL recombinant GST (provided in GST Capture Kit) with a 15 µL injection for a 3 minute contact time. The flow cell was regenerated with a 10 µL injection of Regeneration solution (provided in Amine Coupling Kit) for a 2 minute contact time, leaving captured Recombinant GST on flow cell 2 for reference.

*GST-fusion peptide capture*: GST-peptides E438 and E254 (**Table 2**) were immobilized onto the GST-antibody chip in a modified Hutsell *et al.* protocol (27). The peptides were initially prepared in a 5 µg/mL dilution of running buffer and loaded onto the chip surface at 5 µL/min, increasing concentration and contact time as needed for higher immobilized quantity.

*GST-peptide binding assays*: The analyte peptides N285 and Q444 (**Table 2**) were assayed against their immobilized counter-parts in a serial dilution of concentrations (90 µg/mL, 150 µg/mL, 250 µg/mL, and 359 µg/mL for N285 and 5.8 µg/mL, 11.5 µg/mL, 23.1 µg/mL, and 46.2 µg/mL) for Q444. These assays were run in Tris buffer (50 mM Tris-HCl, 0.4 M NaCl, pH 8.15).

*PIP<sub>2</sub> immobilization*: PtdIns-(4, 5)-P<sub>2</sub>-biotin (biotinylated PIP<sub>2</sub>), obtained from Cayman Chemical (Ann Arbor, Michigan), was immobilized onto a streptavidin (SA) chip. The chip surface was cleaned with three quick pulses of 50 mM NaOH/1M NaCl solution [20 µL injection at 50 µL/min]. The chip was then allowed to stabilize in HBS buffer for 10 minutes. Biotinylated PIP<sub>2</sub> was then loaded [5 µL injection at 5 µL/min] for 200-300 increase in response units (RU's).

*Δ-NT peptide binding assay*: The peptide Δ-NT was assayed against immobilized PIP<sub>2</sub> at concentrations 1 µM, 10 µM, 25 µM, and 50 µM.

## CHAPTER III

### RESULTS AND DISCUSSION

The major goal of this project was to determine potentially critical residues for intersubunit binding of ENaC. The cASIC1 crystal structure, especially using noted areas with high electron density (16), was used to identify residues of possible importance for close intersubunit interactions. Peptides were designed around these residues using the ENaC sequence, and used to assay for any specific binding relationship between the potentially important residues.

#### Identification of potential intersubunit interactions:

In order to begin determination of critical ENaC intersubunit interactions, we first identified potentially important regions to investigate using the crystal structure of cASIC1 (**Figure 6-A**). The search was constrained to residues at the edge of the subunit-subunit barrier, and to residues meeting 3 criteria:

- Relative proximity to opposing subunit residue
- Directionality of R-groups in 2° structure
- R-groups capable of interacting electrostatically (opposing charge / H-bonding)

WT-A6/mut-A6 vs WT-A7: The initial residues identified were found on  $\alpha$ -helices 6 and 7 of adjoining subunits. Upon studying the crystal structure of cASIC1, the

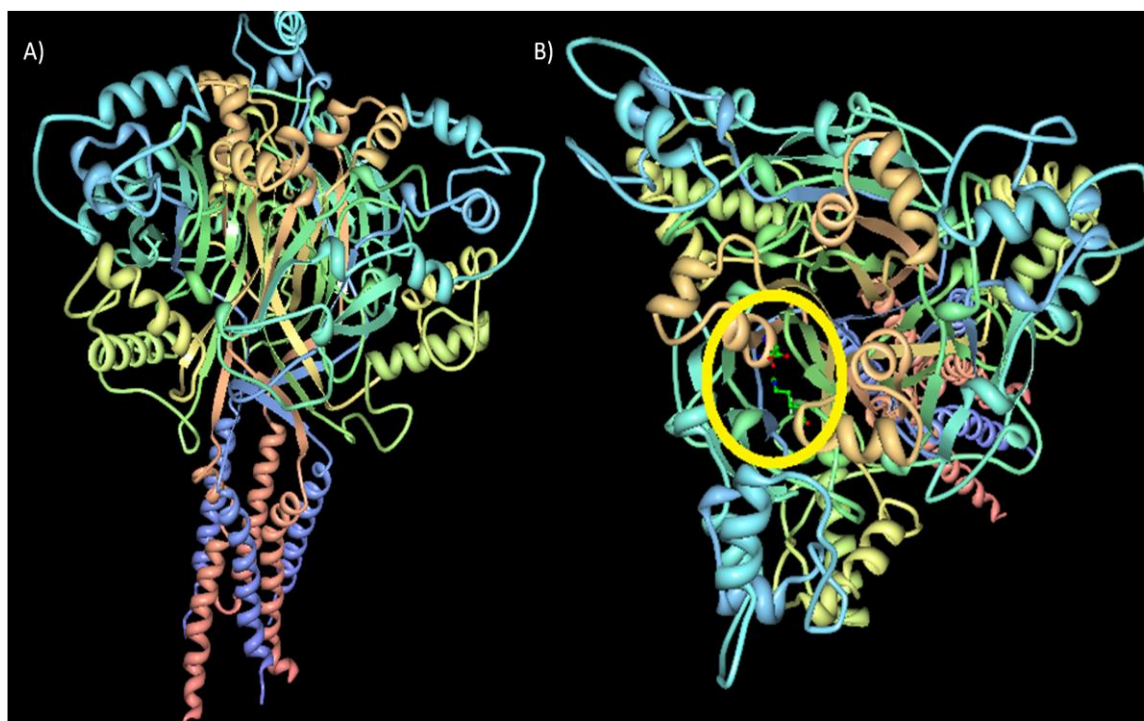


**Figure 6. Crystal structure of chicken ASIC 1.** Protein Data Bank code 2QTS. A) Viewed from the side in Protein Workshop. B) Top view of cASIC1. Residues of the suspect Knuckle-Knuckle interaction are circled. Residues found on Chain A and Chain B.

proximity of these secondary structures subunit-to-subunit, in relation to other residues on opposing subunits, warranted closer investigation. Within the crystal structure, residues lysine 383 of  $\alpha$ -helix 6, chain A, and glutamate 402 of  $\alpha$ -helix 7, chain B, have an appropriate directionality and charge for a possible electrostatic interaction (**Figure 6-B**). The amino acid R-groups of these residues, and their location on their respective secondary structure positioned the charged atoms to be in close proximity to one another. This finding provided a plausible Knuckle-Knuckle interaction for inter-subunit binding. The appropriate ENaC analogue was converted from cASIC1 sequence using the sequence alignment from Stockand *et al.* (14), and a peptide of 12 amino acids encompassing the target residue and immediate 2° structure was designed: WT-A6 (WPSEASEDWIFHV). The glutamate from  $\alpha$ -helix 6 suspected of a strong interaction was

mutated to glycine in a separate peptide for interaction abolishment comparison, labeled as mut-A6 (WPSGASEDWIFHV). The opposing subunit's residue was encompassed in  $\alpha$ -helix 7 peptide and was conjugated with polyethylene glycol (PEG): WT-A7 (NYTVNNKRNGVA). PEG was used to act as a linker, and to separate the ligand from the dextran layer of SPR chip sensor surface.

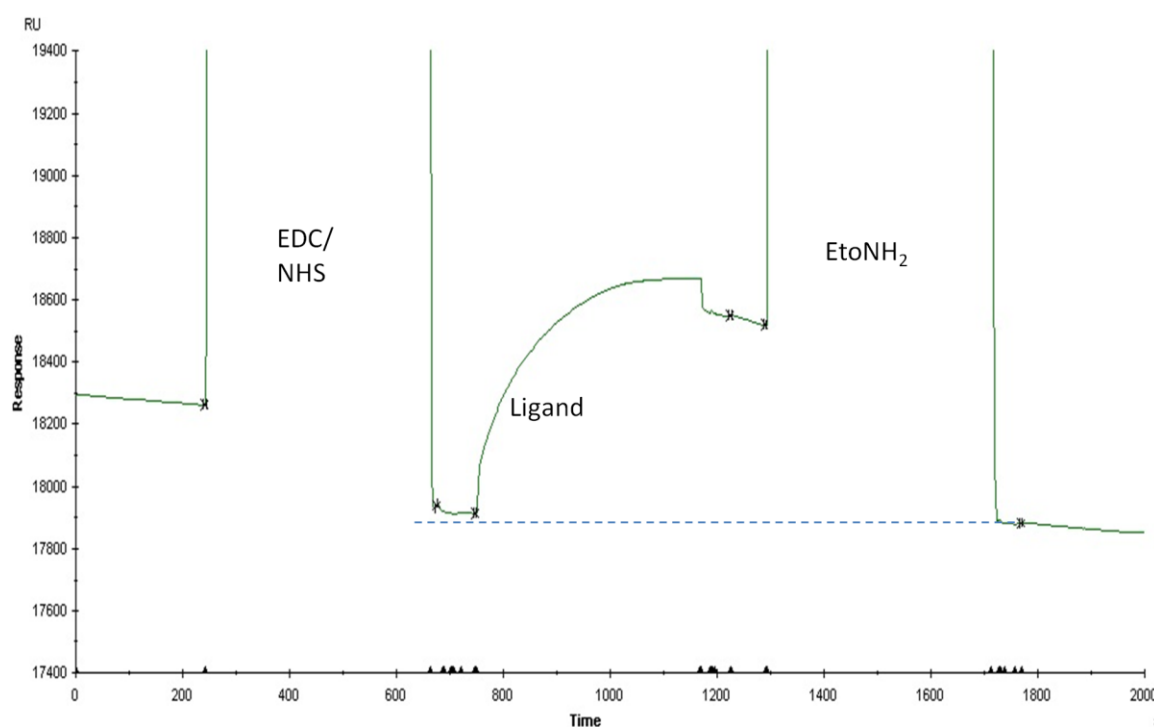


**Figure 7. Immobilization of WT-A7.** WT-A7 (1.5 mM in Na-acetate, pH 4.5 buffer) was flowed over the surface of a CM-5 chip activated with EDC/NHS solution (first peak). The second peak at ~800 seconds is the addition of the ligand WT-47. The final peak at ~1200 seconds is chip surface inactivation with ethanolamine. The dashed line shows that there are no RU's added.

Attempts at Amine coupling of the PEG linked peptide failed (**Figure 7**), but there was still immobilization occurring. An appreciable amount of response units (RU's) on the chip surface remained after injection of the PEG linked peptide, but the amount depreciated continually (**Figure 8**). As regeneration was not an effective means of

removing the immobilized peptide, we deduced that the PEG linker was inserting into the dextran layer, in a pseudo-immobilization, slowly dissociating over time.

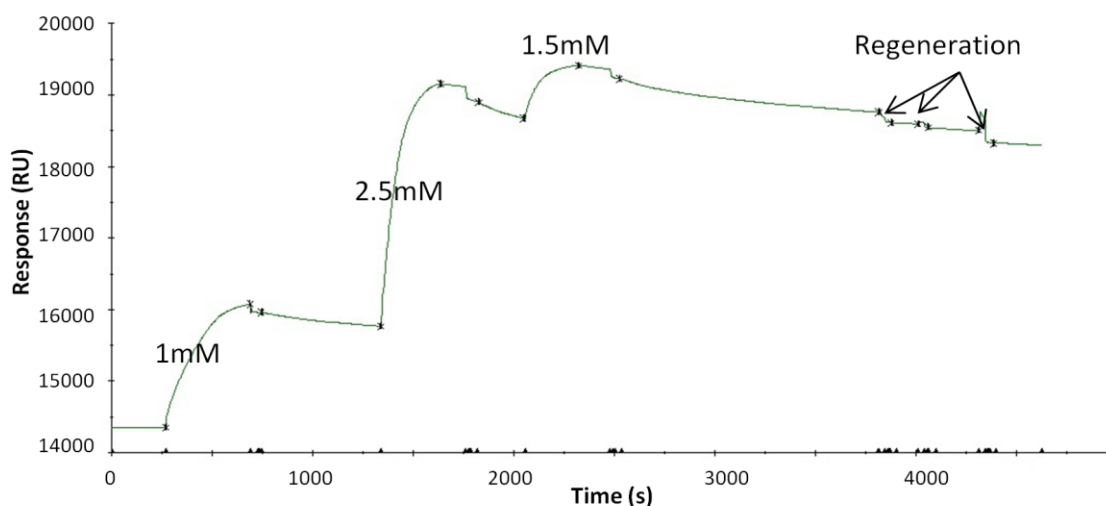


**Figure 8. Immobilization of PEG-WT-A7 via insertion into dextran.** Shown is the immobilization of PEG-WT-A7 via insertion of conjugate PEG into the dextran layer on the CM5 chip surface. The peptide was injected at various concentrations, in order of: 1 mM, 2.5 mM, and 1.5 mM, respective of the first three peaks. Peptide remained associated after wash, indicating insertion. The surface was then regenerated three times, starting at time ~3800s. Regeneration provided very little loss of RU compared to the amount remaining from the injections.

The derivatized ligand (WT-A7) was used in a binding study with serially diluted analyte peptides WT-A6 and mut-A6 (**Figure 9 – A and B**). A comparison of the response observed on the sensorgram revealed a difference between binding patterns of the mutant and wild-type peptides to WT-A7. A proportional increased response was observed relative to concentration of the wild-type peptide, whereas the response observed for the mutant peptide was more static with respect to concentration (**Figure 9**). It is possible that a specific interaction was occurring between WT-A7 and WT-A6 but this needs further investigation.

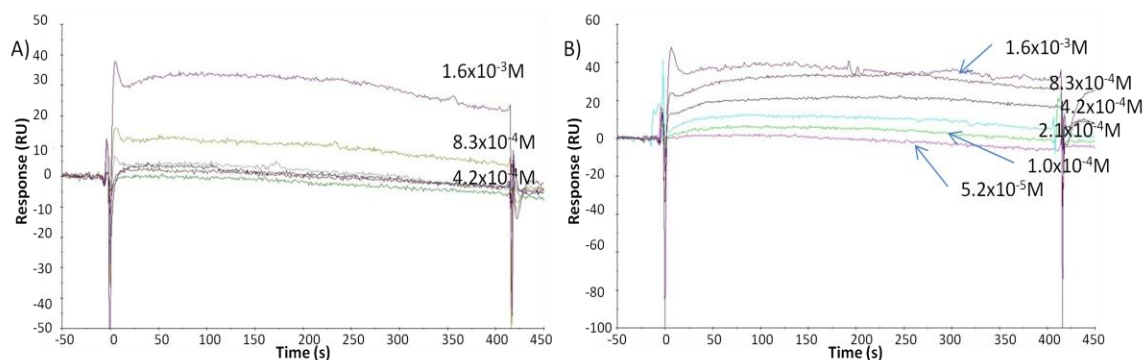


**Figure 9. Serial dilution of analyte against WT-A7.** Sensograms show the reference cell subtracted read-out (peaks overlaid on each other for clarity), with a serial diluted analyte at concentrations  $1.6 \times 10^{-3}$  M,  $8.3 \times 10^{-4}$  M,  $4.2 \times 10^{-4}$  M,  $2.1 \times 10^{-4}$  M,  $1.0 \times 10^{-4}$  M,  $5.2 \times 10^{-5}$  M. Analytes were injected in sample sizes of  $70 \mu\text{L}$  at a flow rate of  $10 \mu\text{L}/\text{min}$ . Sensogram A) is analyte WT-A6, and sensogram B) is analyte mut-A6. For both sensograms, increased injection concentration shows increased peak height.

WT-A7 vs WT-A6: Since the PEGylated peptide did not immobilize appropriately, further studies of these residues required the immobilization of WT-A6 to a CM5 chip (**Figure 10**) and utilization of the peptide WT-A7 as the flow-over analyte. In order to obtain the highest amount of immobilized peptide, the immobilization injection was performed multiple times, starting at  $200 \mu\text{g}/\text{mL}$  and increasing the concentration to  $532 \mu\text{g}/\text{mL}$  on the third injection. After the third injection of WT-A6, the remaining chip surface was re-activated with another application of activation (EDC/NHS) solution, for which three more injections were performed with the peptide. This provided 275 RU's increase from the beginning of the process, corresponding to 275  $\mu\text{g}$  of WT-A6 immobilized on the chip surface.

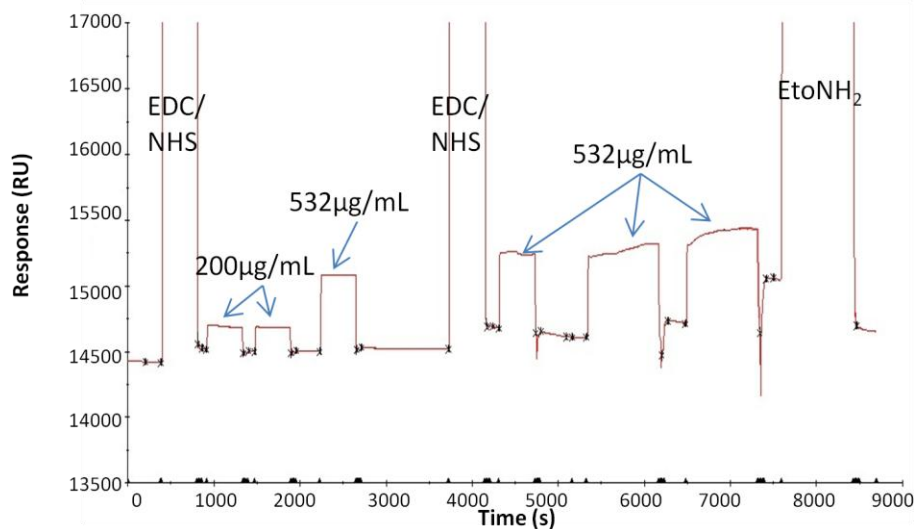


**Figure 10. Derivatization of WT-A6.** Multiple immobilization injections for maximum amount derivatized. EDC/NHS was injected at 390s and 3730s. WT-A6 was injected at an initial concentration of 200  $\mu\text{g}/\text{mL}$ , and then increased to 532  $\mu\text{g}/\text{mL}$  for greater immobilization. The chip surface was sealed with ethanolamine with an injection at 7500s, ultimately leaving  $\sim 145$  RU's immobilized.

An increased association respective to concentration of analyte WT-A7 was observed (**Figure 11**) upon injection of WT-A7 over the surface immobilized with WT-A6. In order to maintain similar ionic strength in the running buffer compared to the peptide solution buffer, the analyte was spiked with 150 mM NaCl. Also, there was a noticeable increase in the RU's of the baseline upon subsequent injections. The slow dissociation observed likely reflects retention of PEG-linked peptide analyte in the dextran layer. However, this is a reference subtracted sensorgram so the increased retention observed relative to that on the reference surface may reflect a specific interaction. Under these conditions, the mutant peptide was not able to be tested, so the abolishment of these interactions cannot be used to verify the nature of the interactions, but warrants further investigation.

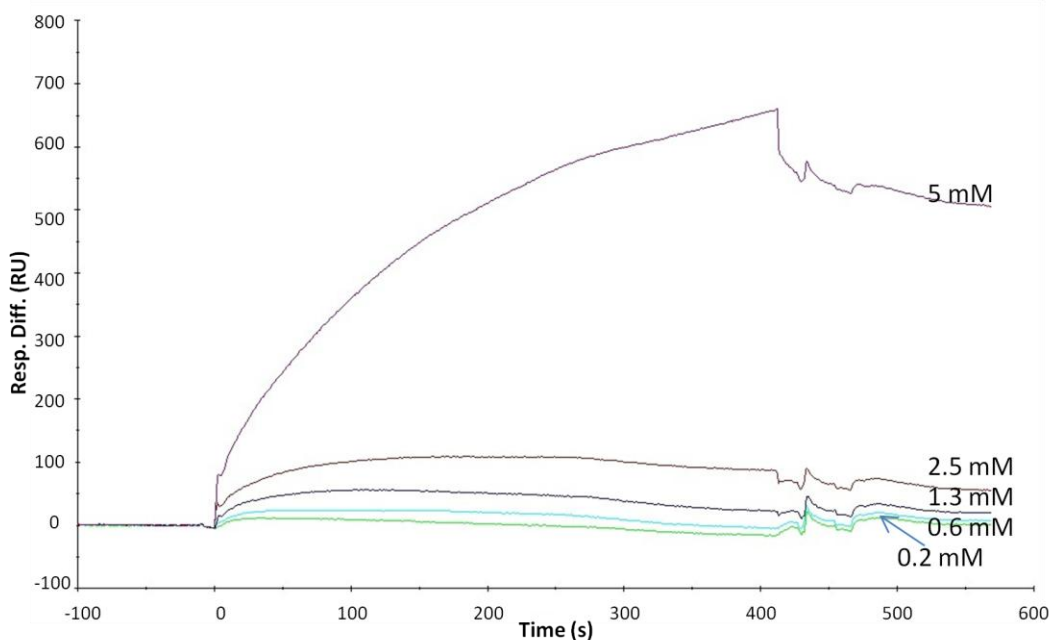


**Figure 11. Serial dilution of analyte against WT-A6.** Shown is an overlay of WT-A7 assayed against WT-A6 in NaCl spiked buffer. Serial dilution concentrations used are, in order of injection: 0.2 mM, 0.3 mM, 0.6 mM, 1.3 mM, 2.5 mM, and 5 mM. Higher concentrations gave successively higher peaks.

In order to more effectively ensure secondary structural integrity of the peptide regions to be investigated for binding interactions, longer peptides were chosen for analysis. Due to the costs associated with commercially obtained peptides, an expression system was devised to produce the desired peptides.

GST-fused peptides:

Peptide design: The X-ray crystallographic data determined by Jasti *et al.* (16) indicated several regions of increased electron density between the subunits that have been inferred as potential interaction points. These are residues that could be enforcing and supporting quaternary structure through binding interactions. In **Table 3**, the hENaC residue for each of these possible interactions, corresponding to those identified as potential interaction points from the cASIC1 crystal structure, was aligned with the

relevant sequential residue from possible adjacent ENaC subunits. Interactions in cASIC1 that are not highlighted do not have corresponding hENaC residues that are probable for interaction, or that could be expressed as peptides for analysis in this study. Since hENaC is heterotrimeric, there are many sequentially relevant residues to consider for possible binding interactions. Highlighted in yellow are residues that, out of the list of corresponding amino acids, have R-groups with electrostatic properties that indicate an interaction may be possible at that location.

**Table 3. Potentially important intersubunit contacts.** cASIC1 Lysine-212 and the corresponding ENaC residues bind to a buried chlorine ion in an adjacent subunit. Residues marked with (?) indicate a residue of cASIC1 located in a portion not located in hENaC, labeled with the next nearest residue in the alignment. Highlighted content indicates cASIC1 residues with the best plausible corresponding hENaC residues (blue), and the specific hENaC residues with best properties to interact (yellow).

Structure		cASIC1		ENaC									
subunit 1	subunit 2	subunit 1	subunit 2	$\alpha$	$\alpha$	$\delta$	$\gamma$	$\delta$	$\alpha$	$\gamma$	$\gamma$	$\alpha$	$\delta$
subunit 1	subunit 2	subunit 1	subunit 2	subunit 1	subunit 2	subunit 1	subunit 2	subunit 1	subunit 2	subunit 1	subunit 2	subunit 1	subunit 2
Palm	Thumb	Arg176	3 carbonyl oxygen (Asn357)	Asn285	His468	Glu438	Glu446	Gly252	His468	Glu446	Asp263	His468	Glu438
Palm	Thumb	Lys212	buried chloride	Met321	Cl-	Cl-	Cl-	Asn288	Cl-	Cl-	Met299	Cl-	Cl-
Palm-loop	Thumb	Glu178	Lys355	Val287	Ser466	Gln436	Gln444	Glu254	Ser466	Gln444	Val265	Ser466	Gln436
Palm-loop	Thumb	Asn217	Arg310	Asn326	Ile417	Leu387	Leu395	Phe293	Ile417	Leu395	Tyr294	Ile417	Leu387
Knuckle	Finger	Tyr388 Lys392	Glu236	Trp502 Met506	Thr345	Ser312	Ser323	Trp471 Val475	Thr345	Ser323	Trp480 Val484	Thr345	Ser312
Knuckle	Finger	Gln271	Glu243	Glu274	Thr347(?)	Ala314(?)	Thr325(?)	Glu341	Thr347(?)	Thr325(?)	Val352	Thr347(?)	Ala314(?)
Wrist/Palm	Wrist/Thumb	Asp79	His74 Gln421	Ile118	Ala113 Glu532	Glu78 Glu503	Thr80 Glu512	Leu83	Ala113 Glu532	Thr80 Glu512	Ile85	Ala113 Glu532	Glu78 Glu503
Wrist/Palm	Wrist/Thumb	Glu80	Tyr283	Asn119	Arg386	Arg353	Lys364	Ser84	Arg386	Lys364	Lys86	Arg386	Arg353

Peptide expression: Preparation of the vector for ligation required digestion at specific sequence sites. The Vector pGEX-4T-2 stock contains an inserted sequence for

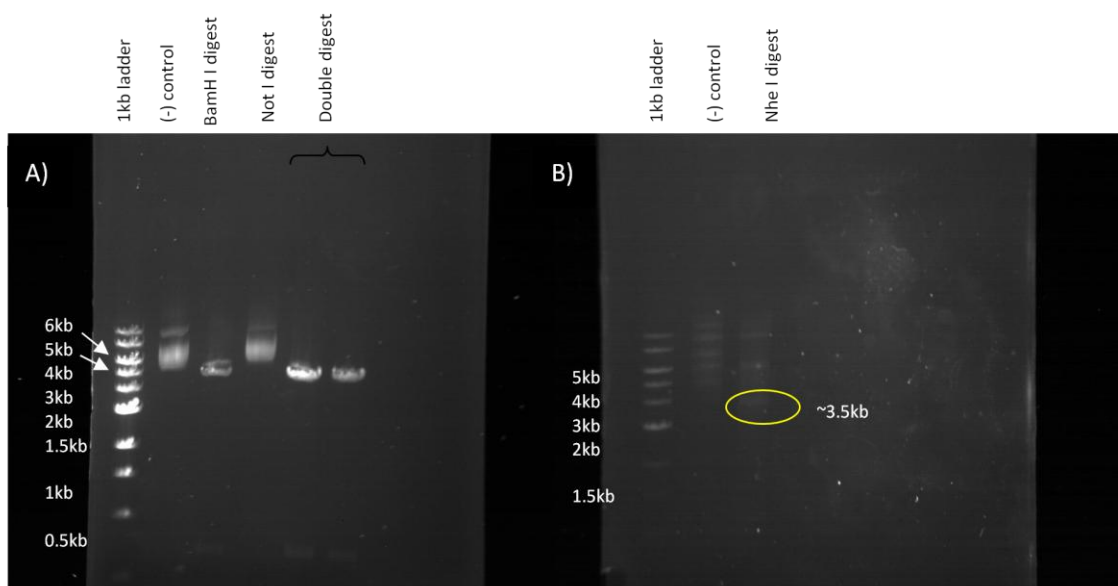


**Figure 12. Digestion of vector.** A) pGEX-4T-2 with hQC inserted, vector digest by Not I and BamH I. B) Nhe I digestion of pLys S from pGEX-4T-2 stocks. The agarose gels were prepared at 1% w/v agarose, and ran with a 1kb ladder, labeled with ethidium bromide.

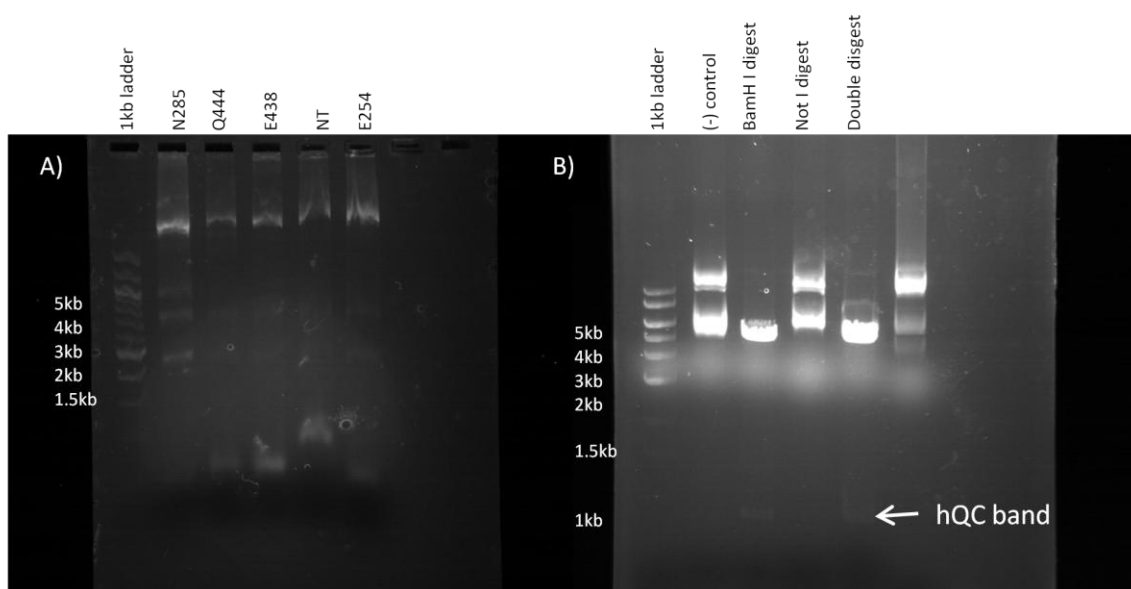


**Figure 13. Insert and vector preparation.** A) Insert double digestion by BamH I and Not I. B) Clean pGEX-4T-2-hQC digestion by BamH I and Not I. Gels prepared as 1% agarose gels, with a 1kb ladder, and stained with ethidium bromide.

hQC, and gives a sum size of about 6000 kilobases, with hQC being 1000 kb. Digestion of the vector with Not I and BamH I showed no digestion (**Figure 12-A**) with Not I. The vector pLys S was mixed in from a previous transformation to BL21. In order to separate the two vectors, pLys S was digested by Nhe I. Nhe I cut pLys S twice, leaving a fragment 3.5 kb in size (**Figure 12-B**); easily visible in the agarose gel along with the clean pGEX-4T-2. Clean pGEX-4T-2 was digested by Not I and BamH I (**Figure 13-B**).

The insert sequences were prepared for ligation through PCR, using primers designed to incorporate in the cut sites Not I and BamH I as per the insertion location in the pGEX-4T-2 vector. The inserts were digested with Not I and BamH I (**Figure 13-A**) in the final preparation for ligation.

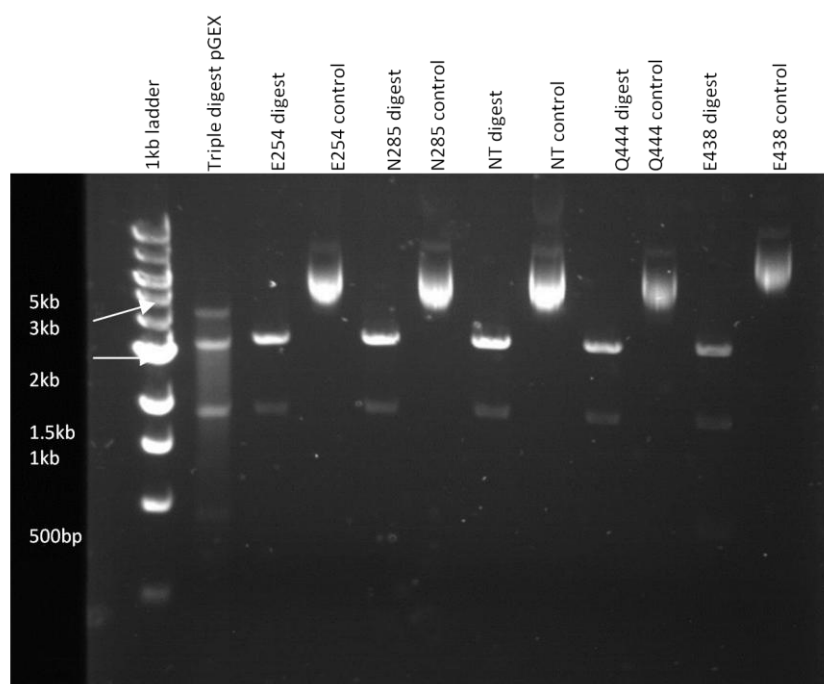


**Figure 14. Ligation product digestion.** Verification of correct ligation with BamH I and BssH II digestion. Gels prepared as 1% agarose gels, with a 1kb ladder, and stained with ethidium bromide.

Ligation was verified through a double digest of ligation products with BamH I and BssH II (**Figure 14**). The ligated pGEX-peptide vector should result in fragments of 3 Kb and 2 Kb when cut with BamH I and BssH II. The initial vector pGEX-4T-2 was cut three times, with BamH I, BssH II, and Not I, for a positive control of the approximate fragment sizes. Along each digested ligation product, an undigested negative control was also run. Bands visible in the digested DNA lanes migrated appropriately for products of 2 Kb and 3 Kb, with expected slight fluctuations pertaining to varying sizes of the insert.

The ligation products were sequentially transformed into Top 10 and BL21 cells. Once the plasmids were transformed into BL21 cells and over-expressed, a crude extract was prepared by lysing the cells with freeze/thaw cycles. The extracts were purified by running them through anti-GST agarose, with the products verified through western blots, and ponceau S staining (**Figure 15-A**). Strong staining was observed in the correct area for migration of the GST-fused peptides.

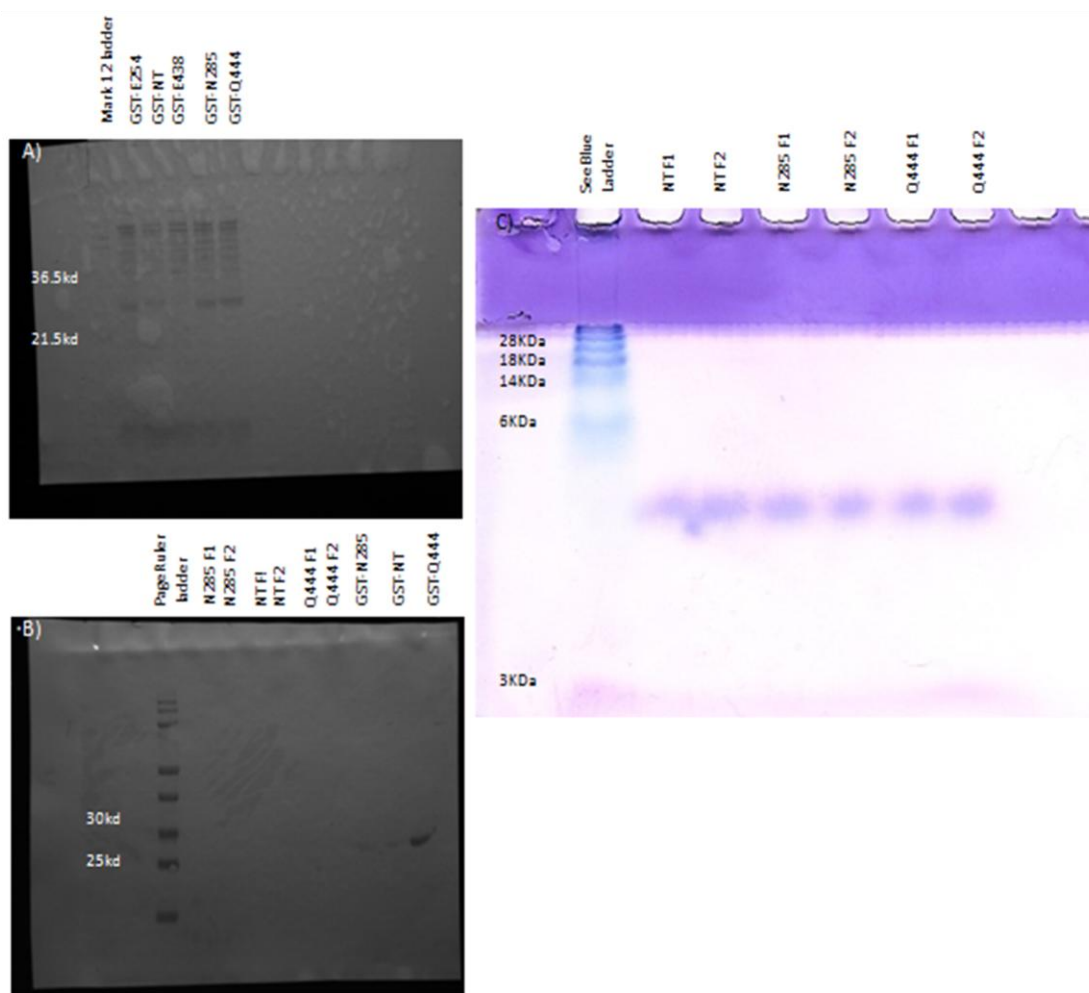


**Figure 15. Expression of GST-fusion peptides.** A) Western blot of expressed GST-tagged fusion peptides, Ponceau S stain. B) Alkaline phosphatase visualization of western blot of GST-tagged/cleaved fusion peptides. C) Coomassie stain of thrombin cleaved peptides.

To prepare the peptides for study with SPR, the GST-fusion peptides N285, Q444, and NT were cleaved from GST with thrombin. The thrombin was then separated from the peptides using *p*-aminobenzamidine, and visualized with a western blot (**Figure 15-B**). The western blot did not show a band corresponding to GST on the cleaved peptides, indicating successful cleavage of GST. Further verification was achieved

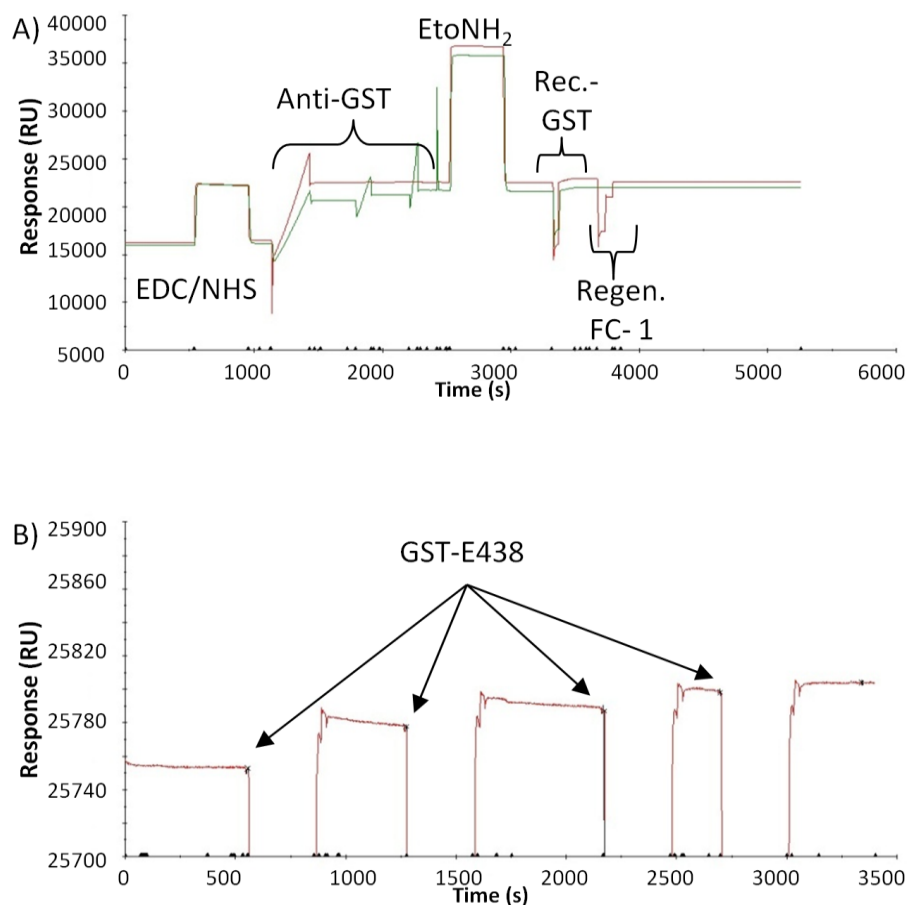


**Figure 16. Immobilization of ligand E438.** A) Sensogram of anti-GST immobilization onto a CM5 sensor chip. Anti-GST injected at 15  $\mu\text{g}/\text{mL}$  for 25  $\mu\text{L}$ . Recombinant GST injected at 5  $\mu\text{g}/\text{mL}$  for 15  $\mu\text{L}$ . B) Final immobilization event of GST-E438 onto captured anti-GST in flow cell 1. GST-E438 injected at a concentration of 5.6  $\text{mg}/\text{mL}$  for 5 minutes of contact time per injection for a total of 275 RU's.

through a 20% tris-tricine gel (**Figure 15-C**) and Coomassie stain. The cleaved peptides migrated as expected for 3-6 KDa size.

*GST-fusion peptide binding assay – E438 vs. N285:* Anti-GST was immobilized onto a CM5 chip via amine coupling. For both analysis and referencing, anti-GST was bound to both flow cells 1 and 2 (**Figure 16-A**). Recombinant GST was used to block any high affinity binding sites in both flow cells, to prevent erroneous readings during

binding assays. An appropriate increase in RU's was observed on flow cell 1 immediately, but flow cell 2 required multiple injections to reach a comparable level. The immobilization captured approximately 6000 pg on flow cell 1 and 5500 pg on flow cell 2. The recombinant GST was removed from the antibody in flow cell 1 by injecting regeneration solution onto flow cell 1 only.

Following immobilization of the anti-GST onto the sensor surface GST-fusion peptide E438 (GST-NRDFPDWAHCYSDLQMSVAQRETCIGMCKES) was captured by

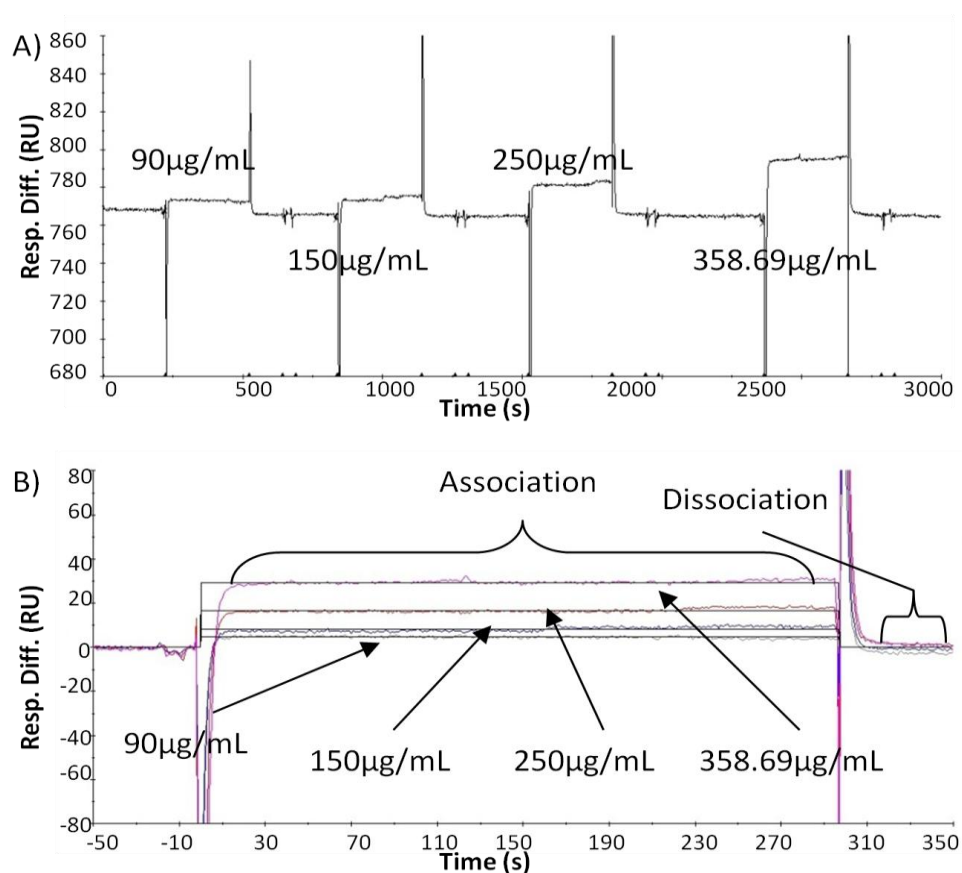


**Figure 17. Binding assay against E438.** A) Binding assay of analyte N285 against bound E438 with concentrations of 90 µg/mL, 150 µg/mL, 250 µg/mL, and 359 µg/mL. Samples run with 50 µL injection at 10 µL/min. B) Kinetic evaluation of binding assay in (A).

multiple injections of the fusion peptide at a concentration of 5.6 mg/mL (**Figure 16-B**). The peptide was captured at an additive total amount of 275 RU's (275 pg of material) over multiple immobilization events (**Figure 16-B**).

Due to differences in the ionic strength of the analyte peptide solution compared to the HBS-EP running buffer, a 50 mM Tris-HCl, 0.4 M NaCl, pH 8.15 buffer was used for subsequent binding studies. The binding assay was conducted using an array of four concentrations of analyte N285 (EDTLGNFIFACRFNQVSCNQANYSHFH): 90, 150, 250, and 359  $\mu\text{g/mL}$ , respectively; using 50  $\mu\text{L}$  injection volume at 10  $\mu\text{L/min}$  (**Figure 17-A**); data was analyzed in BIAevaluation for kinetic evaluation (**Figure 17-B**). An association constant of  $2.03 \times 10^7 \text{ M}^{-1}$  and dissociation constant  $4.93 \times 10^{-8} \text{ M}$  was determined, with a  $\chi^2$  of 1.32. Another run (not shown) under the same conditions gave very similar results of the same order of magnitude with an association constant of  $3.47 \times 10^7 \text{ M}^{-1}$  and a dissociation constant of  $2.88 \times 10^{-8} \text{ M}$  ( $\chi^2 = 1.25$ ) (**Table 4**).

These results indicate a reproducible association event. While the association is not particularly strong, it is observable. This data is in agreement with the interaction being a small part of a larger binding event for the whole subunit. For comparison, a positive control experiment should be run of known peptide interactions to observe similar results. Examples of non-covalent interactions of similar magnitude and strength

between peptides and proteins have been reported (28-31).

**Table 4. E438 Kinetics.** Summary of kinetic values obtained from evaluating GST-fused E438 binding interactions with free N285 in the BIAevaluation program.

$K_a$ (1/Ms)	$K_d$ (1/s)	$K_A$ (1/M)	$K_D$ (M)	$\chi^2$
$1.12 \times 10^3$	$3.22 \times 10^{-5}$	$3.47 \times 10^7$	$2.88 \times 10^{-8}$	1.25

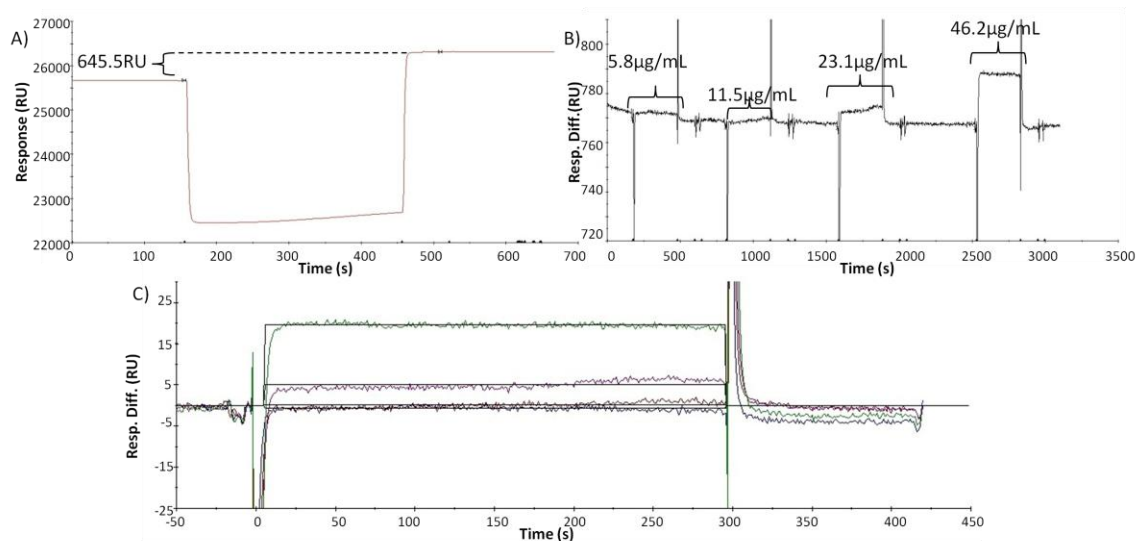


**Figure 18. Binding assay against E254.** A) Immobilization of GST-fused E254 onto anti-GST sensor surface via 25  $\mu$ L injection at 5  $\mu$ L/min flow rate. Produced 645.5 RU's of immobilized peptide. B) Binding assay of GST-E254 to analyte Q444. Assay ran with 50  $\mu$ L injections at 10  $\mu$ L/min, with sample concentrations of 5.8, 11.5, 23.1, and 46.2  $\mu$ g/mL, and a 120s delayed wash. C) Kinetic evaluation of (B) from the BIAevaluation program.

*GST-fusion peptide binding assay – E254 vs. Q444:* Another potential peptide

interaction pair from the list of possible interactions was assayed for binding interactions. This possible interaction involves the residues E178 and K355 from cASIC1, translating to  $\beta$ -palm E254 (SYPGEQMILACLFGAEPNCYRNFTSIFY) and  $\gamma$ -thumb Q444 (YQQHPNWMYCYQLHRAFVQEELGCQSVCKEA), respectively.

GST-fused E254 was captured onto the anti-GST bound sensor chip with a 25  $\mu\text{L}$  injection of 5.6 mg/mL solution, at a flow rate of 5  $\mu\text{L}/\text{min}$ . This produced a response of 645 RU ( $\sim 625$  pg) of immobilized peptide (**Figure 18-A**).

The counter-peptide used as an analyte in this experiment, Q444, had a stock solution with a much lower concentration than achieved with other analytes, therefore, the sample concentrations were notably smaller. On the other hand, Q444 is larger, by almost 1 kDa than N285, so the analyte detection limit was higher, allowing a discernible SPR response at lower concentrations than used in the previous assay.

The binding assay was conducted with a serial dilution of the stock solution of Q444, starting at 46  $\mu\text{g}/\text{mL}$ , and diluting to 23, 11.5, and 5.8  $\mu\text{g}/\text{mL}$ , respectively (**Figure 18-B**). The analyte samples were injected at volumes of 50  $\mu\text{L}$  and a flow rate of 10  $\mu\text{L}/\text{min}$ , with a 120s delayed wash. A relative peak increase was observed to correlate with concentration.

**Table 5. E254 Kinetics.** Summary of kinetic values obtained from evaluating GST-fused E254 binding interactions with free Q444 in the BIAevaluation program.

$K_a$ (1/Ms)	$K_d$ (1/s)	$K_A$ (1/M)	$K_D$ (M)	$\text{Chi}^2$
2.69	$7.41 \times 10^{-5}$	$3.63 \times 10^4$	$2.76 \times 10^{-5}$	1.75

Kinetic evaluation (**Figure 18-C**) of these results gave an association constant of  $3.63 \times 10^4 \text{ M}^{-1}$  and a dissociation constant of  $2.76 \times 10^{-5} \text{ M}$ , at a  $\text{chi}^2$  of 1.75 (**Table 5**).

These numbers indicate an interaction taking place, albeit a weak one, in comparison to that observed between E438 and N285.

*GST-Fusion Peptides Control Assays:* In order to rule out the possibility of a response due to any free GST remaining in the peptide solution from thrombin cleavage during preparation, the binding pattern of GST on both ligand and reference cells was determined. Recombinant GST was used to simulate the free – cleaved GST that could possibly be in the peptide solution, and was injected at concentrations comparable to the amount used to block high affinity sites on anti-GST (1  $\mu\text{g}/\text{mL}$ , 5  $\mu\text{g}/\text{mL}$ , 10  $\mu\text{g}/\text{mL}$ , and 15  $\mu\text{g}/\text{mL}$ ) for 5 minutes of contact time. The binding assay (**Figure 19**) showed a different binding pattern than that of the peptide binding assays, and did not show any dissociation at the end of injection. The lowest concentration injected gave rise to a comparably substantial rise in RUs, and this indicates that the amount of free GST in the peptide solution was negligible. This provides further evidence that the binding interaction of the peptides E438 and N285 is not an artifact.

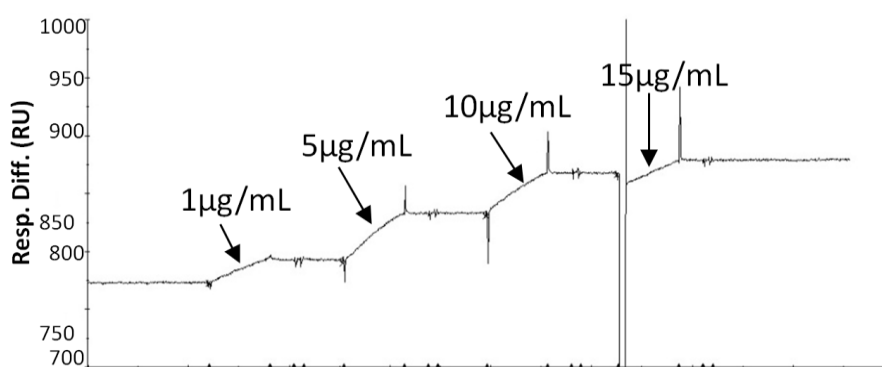


**Figure 19. Free GST control assay.** Assay for effect of free GST against GST-E438 bound to sensor chip. Injected concentrations of 1  $\mu\text{g}/\text{mL}$ , 5  $\mu\text{g}/\text{mL}$ , 10  $\mu\text{g}/\text{mL}$ , and 15  $\mu\text{g}/\text{mL}$  for a 5 minute contact time and 2 minute delayed wash.

In order to validate these results, peptides not expected to participate in any important interaction were assayed together to determine if an observable interaction would occur. The  $\alpha$ -palm peptide N285 was used as an analyte against  $\beta$ -palm peptide GST-E254. Experimentally, this assay was run similarly to the E438 vs. N285 assay with analyte samples of the same concentrations, using the same captured GST-E254 at a level of  $\sim 645$  immobilized RU's.

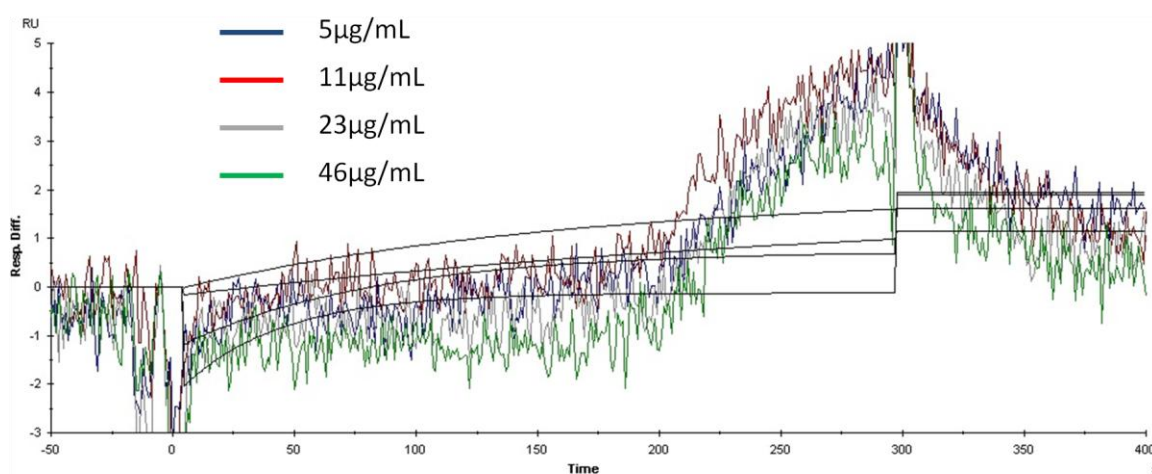


**Figure 20. Non-specific interactions control assay.** Binding assay of non-correlated peptides (palm – palm) N285 to bound E254. Analyte samples were assayed under the same conditions as the E254-Q444 binding study, with at concentrations 5.8, 11.5, 23.1, and 46.2  $\mu\text{g}/\text{mL}$ . A uniform increase in peak height is not seen, and general peak height is very low at about 5 RU's.

Sample injection volumes of 50  $\mu\text{L}$  were used at a flow rate of 10  $\mu\text{L}/\text{min}$  (**Figure 20**). The resulting sensorgram did not show any appreciable response with concentration. A kinetic fit could be forced but the results from this fit are not relevant due to the absence of any real response. A generic non-specific peptide interaction, an unexpected specific interaction between the peptides, or a behavioral interaction pattern from one of the peptides could be present. These peptides are the same as

those used in the previous assays, in which a large discernible response was obtained. However, in this case no interaction was observed, indicating that during the previous experiments specific interactions were observed.

Affector molecule binding:

*β N-terminal peptide vs PIP<sub>2</sub>*: Previous studies performed by other groups have shown an interaction between phosphatidylinositol (4, 5)-bisphosphate (PIP<sub>2</sub>) and a short sequence of amino acid residues on the N-terminal tail of β-ENaC (7). The target sequence is found adjacent to the membrane and is comprised of multiple positive residues with a sequence of [KRIICEGPKKKA]. Even though a definite interaction between β-EnaC and PIP<sub>2</sub> is reported in the literature, it is not clear whether this interaction utilizes cofactors for binding and recognition, or if there is an actual direct binding event between these molecules.

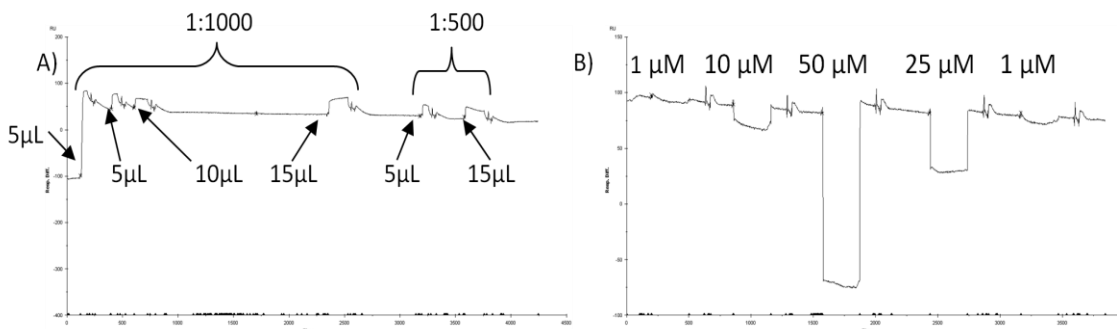


**Figure 21. PIP<sub>2</sub> binding assay.** A) Derivatization of Biotinylated-PIP<sub>2</sub> at 0.9 μM. Labeled are the injection volumes and dilutions of Biotinylated-PIP<sub>2</sub>. Subsequent injections of ligand were performed for higher ligand binding amount. B) Dilutions of Δ-NT-peptide against PIP<sub>2</sub> at concentrations 1 μM, 10 μM, 25 μM, and 50 μM. 50 μL injection volumes were used at a flow rate of 10 μL/min.

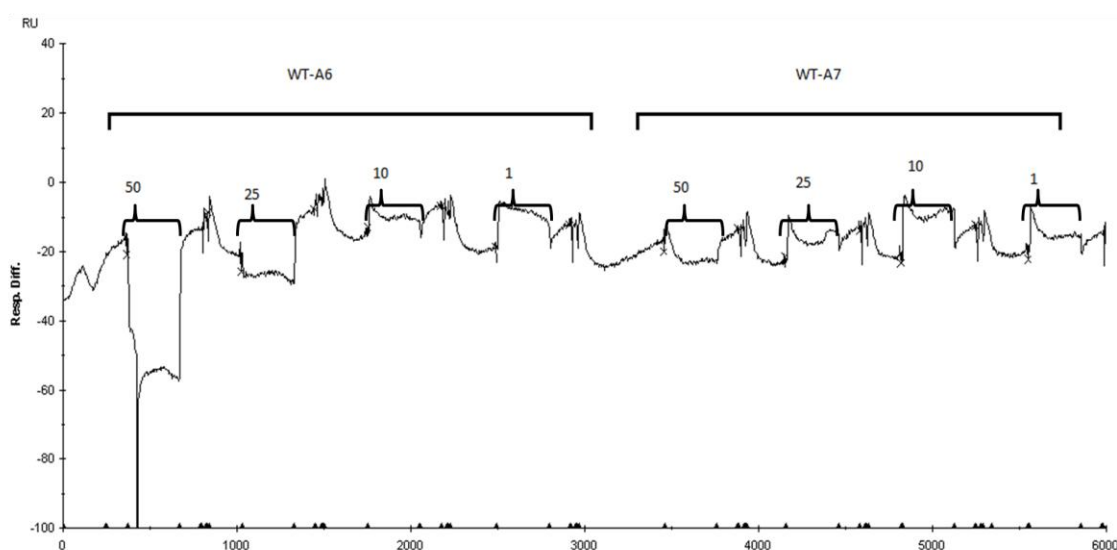


**Figure 22. Non-specific interactions binding assay against PIP<sub>2</sub>.** WT-A6 and WT-A7 against PIP<sub>2</sub>. Analyte concentrations used are 50 μM, 25 μM, 10 μM, and 1 μM. Peptide WT-A6 assayed first, then peptide WT-A7.

Biotinylated-PIP<sub>2</sub> was immobilized onto a streptavidin chip to yield approximately 150 pg of immobilized ligand (**Figure 21-A**). The truncated N-terminal tail peptide (Δ-NT [KRIICEGPKKKA]) was tested in a concentration-dependent manner against the immobilized PIP<sub>2</sub> (**Figure 21-B**). The binding study of the N-terminal tail peptide with PIP<sub>2</sub> showed a negative response in RUs with relation to the concentration, which is, as of yet, for unexplained reasons. Since no effect was observed on the

reference cell indicating a negative shift in RU's due to the injection solution, the observed decrease is a real effect.

As a negative control test, the interactions of PIP<sub>2</sub> were tested with WT-A6 and WT-A7 because there are no expected interactions for those peptides with PIP<sub>2</sub>. At the higher concentration dilutions of peptides, there was still a negative change in RU's (**Figure 22**), but this affect was less pronounced as the dilution increased.

## CHAPTER IV

### CONCLUSION

The human epithelial sodium channel is most likely composed of a 1:1:1 stoichiometry of  $\alpha$ ,  $\beta$ , and  $\gamma$  subunits. Although no crystal structure is available, a model based on cASIC1 has been published. Through thorough study of the predicted structure, and random mutagenesis of potentially critical sequences, intersubunit interactions can be elucidated. In this project a list of plausible residues involved in intersubunit contacts was developed and binding interactions among some of the suspected residues were assayed using SPR.

The interaction between peptides of  $\alpha$ -palm (N285) and  $\beta$ -thumb (E438) was assayed, showing an associative binding pattern with respect to the reference flow cell.

Kinetic evaluation of the interaction gave kinetic constants in range of non-covalent

**Table 6. Summary of Kinetics.** Kinetic values obtained from evaluation of binding assays input into BIAevaluation. This table summarizes the binding affinities found from the individual binding assays. Shown are interactions of peptides  $\alpha$ -palm N285 binding to chip bound  $\beta$ -thumb E438, and  $\gamma$ -thumb Q444 binding to chip bound  $\beta$ -palm E254.

Peptide Interaction	$K_a$ (1/Ms)	$K_d$ (1/s)	$K_A$ (1/M)	$K_D$ (M)	Chi <sup>2</sup>
GST-E438 to N285	$1.12 \times 10^3$	$3.22 \times 10^{-5}$	$3.47 \times 10^7$	$2.88 \times 10^{-8}$	1.25
GST-E254 to Q444	2.69	$7.41 \times 10^{-5}$	$3.63 \times 10^4$	$2.76 \times 10^{-5}$	1.75

interactions (**Table 6**). The interaction between peptides of  $\beta$ -palm (E254) and  $\gamma$ -thumb (Q444) was assayed to give results showing an associative binding pattern as well. Kinetic evaluation of the interaction indicated that this interaction is notably weaker than the previous one observed between  $\alpha$ -palm (N285) and  $\beta$ -thumb (E438), but it is still present (**Table 6**). The immediate next step in characterizing these interactions is to test the bound GST-fused peptides against a full subunit analyte. GST-E438 would require a free  $\alpha$ -subunit, and GST-E254 would require a free  $\gamma$ -subunit. Additionally, these interactions will need to be characterized through an interaction abolishment assay, using point mutations on suspected residues.

Target residues for future study have also been determined (**Table 7**) through the cASIC crystal structure electrodensity residue conversion (**Table 3**).

**Table 7. Future targets.** Selected target residues to continue SPR screen and their location in ENaC (subunit and extracellular domain)

Residue Location	Target residues
$\alpha$ -Knuckle – $\beta$ -Finger	Trp502/Met506 – Ser312
$\beta$ -Wrist/Palm – $\gamma$ -Wrist/Thumb	Ser84 – Lys364

An effector molecule assay was also performed, to try to elucidate and reinforce knowledge on the interaction between the N-terminal tail of  $\beta$ -ENaC and PIP<sub>2</sub>. In order to see if PIP<sub>2</sub> interacts directly with ENaC, or through a cofactor, biotinylated-PIP<sub>2</sub> was bound to a streptavidin sensor chip and a peptide corresponding to the binding site on ENaCs' cytosolic tail was assayed for binding. The sensorgram obtained shows unexplained negative change in RU, respective with concentration of analyte, thus

specific binding information could not be interpreted. As a control, random peptides were assayed against bound PIP<sub>2</sub>, which showed similar negative change in RUs, indicating probable non-specific interactions in the binding pattern. Further study of the interaction will be required to obtain a truer understanding of the PIP<sub>2</sub> – ENaC interaction.

## REFERENCES

1. Garty, H.; Palmer, L. G. Epithelial sodium channels: function, structure, and regulation. *Physiol. Rev.* **1997**, *77*, 359–396.
2. Kellenberger, S.; Schild, L. Epithelial sodium channel/degenerin family of ion channels: a variety of functions for a shared structure. *Physiol. Rev.* **2002**, *82*, 735-767.
3. Kellenberger, S.; Gautschi, I.; Schild, L. Mutations in the Epithelial Na<sup>+</sup> Channel ENaC Outer Pore Disrupt Amiloride Block by Increasing Its Dissociation Rate. *Mol. Pharmacol.* **2003**, *64* (4), 848-856.
4. Nephron - Function and Definition. <http://www.beltina.org/health-dictionary/nephron-function-kidney-definition.html> (accessed June 25, 2012).
5. Oberfeld, B.; Ruffieux-Daidie, D.; Vitagliano, J. J.; Pos, K. M.; Verrey, F.; Staub, O. Disrupt Amiloride Block by Increasing Its Dissociation Rate (ENaC)-ubiquitylating enzyme Nedd4-2. *Am. J. Physiol. Renal Physiol.* **2011**, *301*, F189-F196.
6. Helms, M. N.; Liu, L.; Liang, Y.; Al-Khalili, O.; Vandewalle, A.; Saxena, S.; Eaton, D. C.; Ma, H. Phosphatidylinositol 3,4,5-Trisphosphate Mediates Aldosterone Stimulation of Epithelial Sodium Channel (ENaC) and Interacts with gamma-ENaC. *J. Biol. Chem.* **2005**, *280* (49), 40885–40891.
7. Yue, G.; Malik, B.; Yue, G.; Eaton, D. C. Phosphatidylinositol 4,5-Bisphosphate (PIP<sub>2</sub>) Stimulates Epithelial Sodium Channel Activity in A6 Cells. *J. Biol. Chem.* **2002**, *277*, 11965–11969.
8. Wang, W.; Li, C.; Nejsum, L. N.; Li, H.; Kim, S. W.; Kwon, T.; Jonassen, T. E. N.; Knepper, M. A.; Thomsen, K.; Frokiaer, J.; Nielsen, S. Biphasic effects of ANP infusion in conscious, euvolumic rats: roles of AQP2 and ENaC trafficking. *Am. J. Physiol. Renal Physiol.* **2006**, *290*, F530-F541.
9. Yamada, T.; Konno, N.; Matsuda, K.; Uchiyama, M. Frog atrial natriuretic peptide and cGMP activate amiloride-sensitive Na<sup>(+)</sup> channels in urinary bladder cells of Japanese tree frog, *Hyla japonica*. *J. Comp. Physiol. B* **2007**, *177* (5), 503-508.

10. Asher, C.; Chigaev, A.; Garty, H. Characterization of Interactions between Nedd4 and beta and gamma ENaC using surface plasmon resonance. *Biochem. Biophys. Res. Comm.* **2001**, *286* (5), 1228-1231.
11. Huber, R.; Krueger, B.; Diakov, A.; Korbmacher, J.; Haerteis, S.; Einsiedel, J.; Gmeiner, P.; Azad, A. K.; Cuppens, H.; Cassiman, J. J.; Korbmacher, C.; Rauh, R. Functional Characterization of a Partial Loss-of-Function Mutation of the Epithelial Sodium Channel (ENaC) Associated with Atypical Cystic Fibrosis. *Cell Physiol. Biochem.* **2010**, *25*, 145-158.
12. Canessa, C. M.; Horisberger, J. D.; Rossier, B. C. Epithelial sodium channel related to proteins involved in neurodegeneration. *Nature* **1993**, *361*, 467-470.
13. McNicholas, C. M.; Canessa, C. M. Diversity of channels generated by different combinations of epithelial sodium channel subunits. *J. Gen. Physiol.* **1997**, *109*, 681-692.
14. Stockand, J. D.; Staruschenko, A.; Pochynyuk, O.; Booth, R. E.; Siverthorn, D. U. Insight Toward Epithelial Na<sup>+</sup> Channel Mechanism Revealed by the Acid-sensing Ion Channel 1 Structure. *IUBMB Life* **2008**, *60* (9), 620-628.
15. Giraldez, T.; Rojas, P.; Jou, J.; Flores, C.; Alvarez de la Rosa, D. The epithelial sodium channel  $\delta$  subunit: new notes for an old song. In Press. *Am. J. Physiol. Renal Physiol.* **2012**.
16. Jasti, J.; Furukawa, H.; Gonzales, E. B.; Gouaux, E. Structure of acid-sensing ion channel 1 at 1.9 Å resolution and low pH. *Nature* **2007**, *449*, 316-323.
17. Gessmann, R.; Kourtis, N.; Petratos, K.; Tavernarakis, N. Molecular Modeling of Mechanosensory Ion Channel Structural and Functional Features. *PLoS ONE* **2010**, *5* (9), 1-7.
18. Jiri, H.; Sinclair, S. Y.; Gunter, G. Surface plasmon resonance sensors: review. *Elsevier* **1999**, *54*, 3-15.
19. Antibody-antigen Interactions.  
<http://nfs.unipv.it/nfs/minf/dispense/immunology/agabint.html> (accessed December 5, 2010).
20. Technical Notes: 102 – SPR Sensitivity and Detection Limit.  
[www.biosensingusa.com/application102.html](http://www.biosensingusa.com/application102.html) (accessed July 25, 2012)
21. Sheehan, D. *Physical Biochemistry: Principles and Applications*, 2nd ed.; Wiley-Blackwell: Chichester: West Sussex.
22. *Biacore Sensor Surface Handbook*, AB ed.; General Electric Company, 2005.

23. Swick, A. G.; Janicot, M.; Cheneval-Kastelic, T.; McLenithan, J. C.; Lane, M. D. Promoter-cDNA-directed heterologous protein expression in *Xenopus laevis* oocytes. *Proc. Natl. Acad. Sci. USA* **1992**, *89*, 1812-1816.
24. Chung, C. T.; Miller, R. H. A rapid and convenient method for the preparation and storage of competent bacterial cells. *Nucleic Acids Research* **1988**, *16* (8), 3580.
25. *Current Protocols in Protein Science*; John Wiley & Sons, Inc., 2000.
26. Holleman, W. H.; Weiss, L. J. The Thrombin-like Enzyme from Bothrops atrox Snake Venom: Properties of the Enzyme Purified by Affinity Chromatography on p-Aminobenzamidine-Substituted Agarose. *J. Biol. Chem.* **1976**, *251* (6), 1663-1669.
27. Hutsell, S. Q.; Kimple, R. J.; Siderovski, D. P.; Willard, F. S.; Kimple, A. J. High affinity immobilization of proteins using biotin- and GST- based coupling strategies. *Methods Mol. Biol.* **2010**, *625*, 75-90.
28. Nogues, C.; Leh, H.; Langendorf, C. G.; Law, R. H. P.; Buckle, A. M.; Buckle, M. Characterisation of Peptide Microarrays for Studying Antibody-Antigen Binding Using Surface Plasmon Resonance Imagery. *PLoS ONE* **2010**, *5* (8).
29. Cohavi, O.; Reichmann, D.; Abramovich, R.; Tesler, A. B.; Bellapadrona, G.; Kokh, D. B.; Wade, R. C.; Vaskevich, A.; Rubinstein, I.; Schreiber, G. A Quantitative, Real-Time Assessment of Binding of Peptides and Proteins to Gold Surfaces. *Chem. Eur. J.* **2011**, *17* (4), 1327-1336.
30. Geitmann, M.; Dahl, G.; Danielson, U. H. Mechanistic and kinetic characterization of hepatitis C virus NS3 protein interactions with NS4A and protease inhibitors. *J. Mol. Recognit.* **2010**, *24* (1), 60-70.
31. Stabenfeldt, S. E.; Gossett, J. J.; Barker, T. H. Building better fibrin knob mimics: an investigation of synthetic fibrin knob peptide structures in solution and their dynamic binding with fibrinogen/fibrin holes. *Blood* **2010**, *116* (8), 1352-1359.

## VITA

Grantham Chase Peltier was born in Houston, Texas on October 24<sup>th</sup>, 1986, the son of Arthur M. Peltier and Susan G. Peltier. He attended and graduated from Tomball High School, in Tomball, Texas in 2005. He then entered Texas A&M at College Station, Texas, where he received a degree of Bachelor of Science in Biochemistry. He then enrolled in the Graduate College of Texas State University-San Marcos to pursue his post-baccalaureate work in biochemistry.

Permanent Address:           23140 Jane Road  
  
                                          Tomball, TX 77377

This Thesis was typed by Grantham C. Peltier